HOPF BIFURCATIONS AND LIMIT CYCLES IN EVOLUTIONARY NETWORK DYNAMICS [*]

DARREN PAIS[†], CARLOS H. CAICEDO-NÚÑEZ[†], AND NAOMI E. LEONARD[†]

Abstract. The replicator-mutator equations from evolutionary dynamics serve as a model for the evolution of language, behavioral dynamics in social networks, and decision-making dynamics in networked multi-agent systems. Analysis of the stable equilibria of these dynamics has been a focus in the literature, where symmetry in fitness functions is typically assumed. We explore asymmetry in fitness and show that the replicator-mutator equations exhibit Hopf bifurcations and limit cycles. We prove conditions for the existence of stable limit cycles arising from multiple distinct Hopf bifurcations of the dynamics in the case of circulant fitness matrices. In the noncirculant case we illustrate how stable limit cycles of the dynamics are coupled to embedded directed cycles in the payoff graph. These cycles correspond to oscillations of grammar dominance in language evolution and to oscillations in behavioral preferences in social networks; for decision-making systems, these limit cycles correspond to sustained oscillations in decisions across the group.

Key words. replicator-mutator dynamics, limit cycle bifurcations, social networks

AMS subject classifications. 91A22, 37G15, 91D30

1. Introduction. Evolutionary dynamics [32, 19, 7, 31] are, broadly speaking, an effort to cast the basic tenets of Darwinian natural selection (replication, competition, strategy dependent fitness, mutation) in a mathematical framework that can be simulated, interpreted, and often rigorously analyzed. John Maynard Smith's pioneering work [25] made formal connections between classical game theory and evolutionary dynamics. Particularly important was Maynard Smith's definition of evolutionarily stable strategies (ESS's), which are equilibria of an evolutionary dynamical system that are uninvadable by other competing strategies in the environment, and hence stable in an evolutionary sense. From a game theoretic perspective, ESS's are a subset of the Nash equilibria of a game: they satisfy both the Nash best reply condition and evolutionary uninvadability.

The replicator dynamics [27] are the simplest model of evolutionary dynamics for a large population comprised of N sub-populations, each subscribed to a different competing strategy. These differential equations model the game theoretic interactions among the sub-populations and determine how each sub-population changes in size as a consequence of these interactions. Lyapunov stable equilibria of the replicator dynamics are Nash equilibria of the corresponding game [34]. Further, all ESS's of the replicator dynamics are asymptotically stable [34].

Although the replicator dynamics have proved to be a powerful tool in analyzing a variety of classical games from an evolutionary perspective, they do not model mutation, a key ingredient of selection theory. Mutation can be included by adding the possibility that individuals spontaneously change from one strategy to another. This yields the replicator-mutator dynamics [2, 21], which have played a prominent role in evolutionary theory and contain as limiting cases many other important equations in biology [10]; these include models of language evolution [17], autocatalytic reaction networks [26], and populations genetics [5]. The dynamics have also recently been

[†]Department of Mechanical and Aerospace Engineering, Princeton University, Princeton, NJ 08544, USA ({dpais, ccaicedo, naomi}@princeton.edu).

employed to model social and multi-agent network interactions [20]. The replicator-mutator equations have been shown in [21] to be equivalent to the generalized Price equation from evolutionary genetics [23, 24]. The standard replicator dynamics can be obtained from the replicator-mutator dynamics in the limit of zero mutation.

In this paper we study a form of the replicator-mutator dynamics and prove conditions for Hopf bifurcations and stable limit cycles for $N \geq 3$ competing strategies. Stable limit cycles correspond to sustained oscillations in strategy dominance across some or all of the population. The form of the dynamics considered, and the interpretation of the oscillations, depends on the applications of interest; the following are three motivating applications.

a) The replicator-mutator dynamics have been used in the development of a mathematical framework for the evolution of language [17]. For a large population, the strategies represent different grammars in the population and mutations reflect errors in grammar transmission or learning from one generation to the next. A key result is the bifurcation of the equilibria from a state where several grammars coexist in a population to a state of high grammatical coherence as mutations in the population decrease (or equivalently, the fidelity of learning increases) [12, 3, 15]. Limit cycles of the replicator-mutator dynamics correspond to oscillations in the dominance of the different grammars in the population. As noted in [16], oscillations appear to be more realistic than stable equilibria for the language dynamics with timescales on the order of several centuries.

b) The replicator-mutator dynamics were recently proposed [20, 9] as a model for behavior adoption in social networks, with a focus on the emergence of dominance of particular behaviors in these networks. Simulations of the evolutionary social network model show a shift from the dominance of a single strategy (behavior), to the coexistence of a few strategies, to eventually the collapse of dominance, as the extent of mutation in the network increases. Limit cycles of the replicator-mutator dynamics correspond to oscillations of behavior preference in this context, for example cycles in trends or fashions.

c) The replicator-mutator dynamics can also be used to model decision-making dynamics in networked multi-agent systems. It has been shown that simple models with pairwise interactions between agents and noisy imitation of successful strategies evaluate (under certain conditions) to the replicator-mutator dynamics [6, 1, 30, 29]. Recent papers have employed the replicator-mutator equations to model wireless multi-agent networks [33, 28]. Hopf bifurcations of replicator-mutator dynamics in this context address the exploration versus exploitation trade-off: few mutations favor fast convergence to a decision (exploitation) whereas extensive mutations favor exploration of the decision space. In an intermediate range, mutations can lead to limit cycles, which enable dynamic examination of alternative choices.

The analysis of the replicator-mutator dynamics in the literature has focused primarily on stable limiting equilibrium behavior where the fitness terms are assumed to have a lot of symmetry (e.g. [3, 17, 20]). However, the recent $N = 2$ analysis in [11] shows that the symmetric case is structurally unstable and that breaking symmetry in fitness yields qualitatively different bifurcations of the dynamics. Further, in [16] the authors illustrate that the replicator-mutator dynamics exhibit limit cycles and chaos for specific model parameter values.

In this paper, we show that the limiting behaviors of the replicator-mutator dynamics are tied to the structure of the fitness model, and we prove how breaking

symmetry yields some of the richer outcomes simulated in [16]. It is known that the replicator dynamics for $N \geq 4$ can generate limit cycles and chaos for particular choices of fitness [16, 26, 18]. Here we investigate the role that both fitness and mutation play in generating limit cycles for the replicator-mutator dynamics. With mutation strength as the bifurcation parameter, we prove Hopf bifurcations for the replicator-mutator dynamics with $N \geq 3$ and characterize the existence of stable limit cycles using an analytical derivation of the Hopf bifurcations points and the corresponding first Lyapunov coefficients [4, 13]. We focus on a class of circulant fitness matrices for our analytical calculations, and explore bifurcations and limit cycles for more general non-circulant fitness matrices using simulations. While circulant fitness matrices may be explicitly relevant for the applications identified, we also expect that more general fitness matrices are relevant. Accordingly, we motivate our focus on circulant matrices as a step towards better understanding the influence of cycles in the more general cases.

In §2 we provide the details of the replicator-mutator dynamics and the simplex phase space on which the dynamics evolve. In §3 we show motivating simulations and illustrate bifurcations of the dynamics for $N = 3$ strategies, summarizing our previous work in [22]. In §4 we present our main result proving Hopf bifurcations for $N \geq 3$ strategies and a two-parameter family of circulant fitness matrices. We examine one-parameter circulant fitness matrices in §5 and consider noncirculant cases in §6. In §7 we conclude and discuss future directions.

2. Replicator-Mutator Dynamics. Consider a large population of agents and N distinct strategies S_i, $i = 1, 2, \cdots, N$. Let strategy frequency $x_i \in [0, 1]$ be the fraction of individuals in the population with strategy S_i such that $\sum_{i=1}^{N} x_i = 1$. Let the population distribution vector $\boldsymbol{x} = [x_1, \cdots, x_N]^T$. The fitness f_i of agents with strategy S_i is given by

$$f_i = \sum_{k=1}^{N} b_{ik} x_k.$$

Let $\boldsymbol{f} = [f_1, \cdots, f_N]^T$. Then $\boldsymbol{f} = B\boldsymbol{x}$, where $B = [b_{ij}] \in \mathbb{R}^{N \times N}$, and the average population fitness is $\phi = \boldsymbol{f}^T \boldsymbol{x} = \boldsymbol{x}^T B \boldsymbol{x}$. B is known as the payoff matrix where $b_{ij} \geq 0$ represents the payoff to an agent with strategy S_i on interacting with an agent with strategy S_j.

We assume that payoffs are all non-negative and that agents get a maximal payoff (normalized to 1) on interacting with others subscribed to the same strategy. Hence B satisfies

$$b_{ii} = 1 \text{ and } b_{ij} \in [0, 1) \text{ for } i \neq j. \tag{2.1}$$

As noted in [20], the payoff matrix B can be interpreted from a graph theoretic perspective as the adjacency matrix of a directed graph. The nodes of the graph correspond to the strategies S_i. The diagonal elements of B ($b_{ii} = 1$) correspond to self-cycles at each node. Each of the non-zero off-diagonal elements b_{ij} corresponds to the weight of a directed edge from node S_i to node S_j. Symmetric payoff matrices B correspond to undirected graphs. This graph theoretic viewpoint is important in our work, particularly as a tool to visualize the structure of the payoff matrix. Consider the following condition:

CONDITION 1. *Every row and column of B has at least one non-zero off diagonal element.*

From the graph theoretic perspective, Condition 1 requires that every node of the graph has at least one outgoing and one incoming link; this ensures that there are no isolated disconnected nodes of the payoff graph. We will restrict to examining graphs that satisfy Condition 1.

Next we define q_{ij} to be the probability that agents with strategy S_i mutate (spontaneously change) to strategy S_j. Note that since $\sum_j q_{ij} = 1$, the mutation matrix $Q = [q_{ij}]$ is row stochastic. The elements of the mutation matrix Q are defined in terms of a mutation parameter $\mu \in [0, 1]$. The mutation parameter represents the probability of error in replication. For example, $\mu = 0$ denotes perfect replication and no mutation whereas $\mu = 1$ denotes pure mutation.

In this paper, we use two specific models for the mutation matrix Q. The first model defines the mutation probabilities q_{ij} as a function of the payoffs b_{ij} and the mutation strength μ as follows:

$$q_{ii} = (1 - \mu), \quad q_{ij} = \frac{\mu b_{ij}}{\sum_{i \neq j} b_{ij}} \text{ for } i \neq j. \tag{Q1}$$

The form of q_{ij} in (Q1) is motivated by the graph theoretic perspective on the replicator-mutator dynamics and is a generalization of the structured mutational models in [14, 11]. Intuitively, this model implies that spontaneous mutation to alternative strategies is weighted in favor of strategies that yield higher payoff. The mutation models in [20, 14, 3, 17] are special cases of (Q1) in which the payoff matrix B is symmetric. We call (Q1) the *dependent* mutation model since (Q1) is dependent on B.

The second mutation model we consider corresponds to a uniform random probability of mutating to alternative strategies as follows:

$$q_{ii} = (1 - \mu), \quad q_{ij} = \frac{\mu}{N - 1} \text{ for } i \neq j. \tag{Q2}$$

We call (Q2) the *independent* mutation model since (Q2) is independent of B.

There are several alternative possibilities for the mutation matrix Q. Our choice of (Q1) and (Q2) enables a comparison between independent and dependent mutation models, and represents two generic models that are popular in the literature and meaningful in the context of our motivating applications.

The strategies S_i, payoffs b_{ij} and mutation probabilities q_{ij} can be interpreted in each of our motivating contexts:

a) For the evolution of language, each S_i is a specific grammar in the population and b_{ij} is the probability that a sentence spoken at random by individuals with grammar S_j can be parsed by individuals with grammar S_i. Higher values of the diagonal terms $q_{ii} = 1 - \mu$ of the mutation matrix Q correspond to more effective language transmission or learning, and the off-diagonal terms q_{ij} correspond to mutation probabilities to alternative grammars.

b) In social networks, each S_i represents a particular behavior in a population and b_{ij} represents the degree to which agents with behavior S_i are attracted to behavior S_j. Higher values of the mutation probabilities q_{ij} correspond to a greater tendency for individuals to explore and adopt alternative behaviors in the population.

c) In multi-agent decision making, each S_i represents an alternative choice for the group and the b_{ij} represent the perceived relative advantage of choice S_j for agents currently subscribed to choice S_i. The mutation terms q_{ij} model errors in the decision-making process.

The replicator-mutator dynamics describe the dynamics of the population distribution $\boldsymbol{x}$ as a result of replication driven by fitness $\boldsymbol{f}$ and mutation driven by Q:

$$\dot{x}_i = \sum_{j=1}^{N} x_j f_j(\boldsymbol{x}) q_{ji} - x_i \phi =: g_i(\boldsymbol{x}); \quad \phi = \boldsymbol{f}^T \boldsymbol{x}. \tag{2.2}$$

The replicator-mutator dynamics (2.2) can be derived as the limit of a simple stochastic error-prone imitation process, where agents imitate successful strategies proportional to relative payoffs (f_i/ϕ) and mutate to alternative strategies with probabilities q_{ij}; see [6, 1, 30] for details. As illustrated in [30, 1], there exist several possible microscopic imitation mechanisms that yield alternatives to the replicator-mutator dynamics in the limit. For this paper, we focus on the replicator-mutator dynamics as these are popular in the literature and hence allow for comparisons with past work [3, 20, 14, 16].

The dynamics (2.2) evolve on the $(N-1)$-dimensional simplex phase space as follows. Define the n-simplex as

$$\Delta_n = \left\{ \boldsymbol{x} \in \mathbb{R}^{n+1} \mid x_i \geq 0, \ \boldsymbol{x}^T \boldsymbol{1} = 1 \right\},$$

where $\boldsymbol{1}$ is a column vector of ones of appropriate dimension. Let $\boldsymbol{g}(\boldsymbol{x}) : \mathbb{R}^N \to \mathbb{R}^N$ be $\boldsymbol{g}(\boldsymbol{x}) = [g_1(\boldsymbol{x}), \cdots, g_N(\boldsymbol{x})]^T$ where $g_i(\boldsymbol{x})$ is defined in (2.2). One can compute directly from (2.2) that $\boldsymbol{x}^T \boldsymbol{1} = 1 \implies \boldsymbol{1}^T \boldsymbol{g}(\boldsymbol{x}) = \boldsymbol{0}$. Hence $\boldsymbol{x}^T \boldsymbol{1} = 1$ is an invariant hyperplane for the dynamics. Further, the non-negative orthant of $\mathbb{R}^N$ is a trapping region for the dynamics; this follows from the fact that $\dot{x}_i|_{x_i=0} \geq 0$. The intersection of the invariant hyperplane and the non-negative orthant of $\mathbb{R}^N$ is the simplex Δ_{N-1}. Hence Δ_{N-1} is a trapping region for the replicator-mutator dynamics (2.2).

Given the restriction to the simplex Δ_{N-1}, the N-dimensional dynamics (2.2) can be reduced to an $(N-1)$-dimensional system of equations:

$$\dot{x}_i = h_i(\tilde{\boldsymbol{x}}), \ \ i \in \{1, 2, \cdots, N-1\},$$
$$h_i(\tilde{\boldsymbol{x}}) := g_i \left(x_1, x_2, \cdots, x_{N-1}, 1 - \sum_{j=1}^{N-1} x_j \right), \tag{2.3}$$

where $\tilde{\boldsymbol{x}} = [x_1, \cdots, x_{N-1}]^T$ and $\boldsymbol{h} : \mathbb{R}^{N-1} \to \mathbb{R}^{N-1}$.

3. Motivating Simulations and Analysis. Our motivation to prove the existence of limit cycles in replicator-mutator dynamics comes in part from simulations of the dynamics (2.2) for random payoff matrices B (b_{ij} chosen from the uniform distribution on the interval $[0, 1)$ for $i \neq j$), which frequently exhibit oscillations. Figure 3.1 shows one simulation of the dynamics that is typical for mutation matrix (Q1) or (Q2). The dynamics in this simulation illustrate the shift from dominance of a single strategy (Figure 3.1(a)), to the coexistence of several strategies (Figure 3.1(b)), to eventually the collapse of dominance (Figure 3.1(c)), as the extent of mutation (parameterized by μ) increases. The study of the collapse of dominance, as a consequence of a bifurcation in the dynamics, has received significant attention in the literature (e.g. [3, 17, 12, 14]).
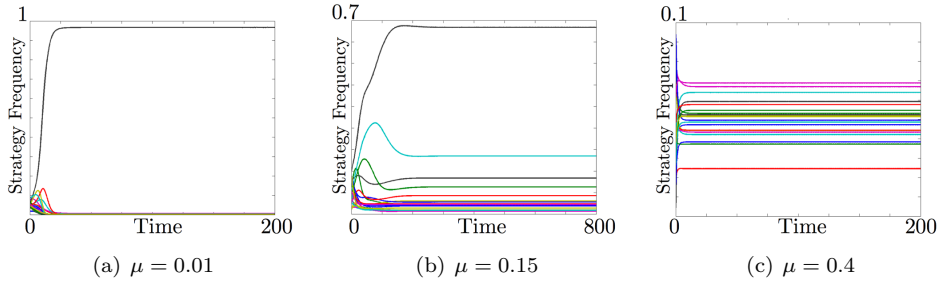
(a) $\mu = 0.01$ (b) $\mu = 0.15$ (c) $\mu = 0.4$

FIG. 3.1. *A first typical simulation of the dynamics (2.2) for $N = 20$ nodes and $b_{ij} \in [0, 1)$ chosen randomly from the uniform distribution. The dynamics shift from (a) a highly coherent state for small μ, to (b) a less coherent state for intermediate μ, and eventually collapse to (c) a mixed state for large μ.*

Figure 3.2 shows another simulation of the replicator-mutator dynamics that is also typical for mutation matrix (Q1) or (Q2). The dynamics in this simulation also transition from dominance of a single strategy (Figure 3.2(a)) to collapse of dominance (Figure 3.2(c)). However, unlike the first simulation, the dynamics exhibit sustained oscillations in strategy dominance at intermediate values of mutation strength μ (Figure 3.2(b)). In [16], the authors consider specific asymmetric payoff matrices and, using simulations, illustrate stable limit cycles for the replicator-mutator dynamics that result.
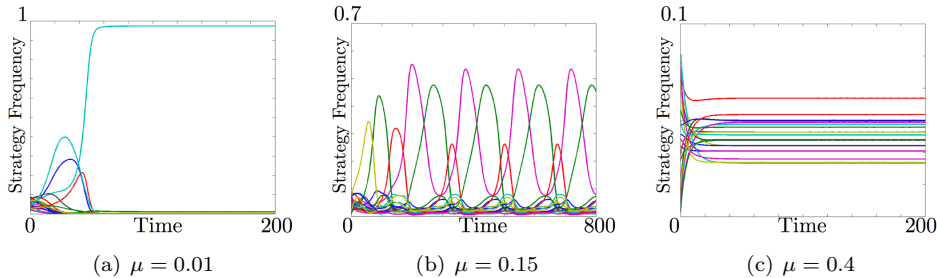

(a) $\mu = 0.01$ (b) $\mu = 0.15$ (c) $\mu = 0.4$

FIG. 3.2. *A second typical simulation of the dynamics (2.2) for $N = 20$ nodes and $b_{ij} \in [0, 1)$ chosen randomly from the uniform distribution. The dynamics transition from (a) a highly coherent state for small μ, to (b) oscillating dominance for intermediate μ, and eventually to (c) a mixed collapse of dominance for large μ.*

3.1. Analysis for $N = 3$ Strategies. To build intuition for our general results in §4, we summarize here the main results from our recent paper [22], which focuses on the bifurcations of the dynamics (2.2) as a function of the bifurcation parameter μ for $N = 3$ strategies. Because the simplex is two-dimensional for $N = 3$ (2.3), it is easier than in higher dimensions to prove necessary and sufficient conditions for limit cycles and to visualize codimension-one bifurcations. We show a transition from multiple stable dominant equilibria to a unique stable mixed equilibrium for increasing μ, and prove conditions for stable limit cycles to exist over an intermediate range of μ.

Consider the dynamics (2.2) with $N = 3$ and with the payoff parameters b_{ij} in (2.1) set to be either 0 or equal to a constant value $b > 0$. There are five non-isomorphic graph topologies with three nodes that satisfy the connectivity specified by Condition 1 and have edges of identical weight b; these are shown in Figure 3.3.

Figure 3.3 also shows the analytically computed[1] bifurcation plots for each of the topologies as a function of the mutation strength μ for mutation matrix (Q1) and payoff matrix (2.1). The corresponding plots for mutation matrix (Q2) are shown in Figure 3.4.
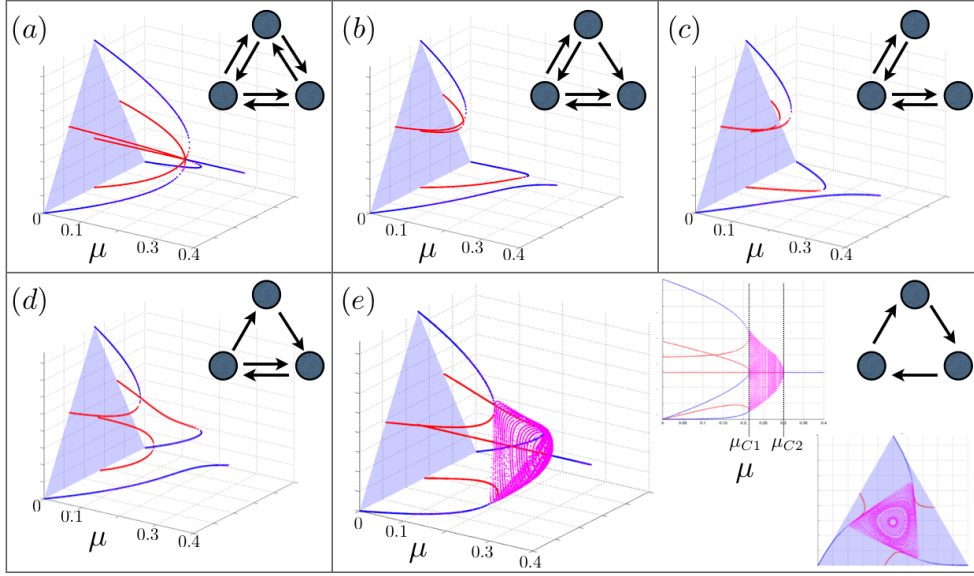

FIG. 3.3. *Bifurcation plots for the $N = 3$ case of dynamics* (2.2), *constant edge weights $b = 0.2$ and mutation matrix* (Q1). *The x-axis in each plot is the mutation strength μ, blue and red curves are stable and unstable equilibria, respectively, and the magenta curves are stable limit cycles. The three-node graphs in each subplot have adjacency matrix B with self-cycles (not shown) at each node.*

FIG. 3.4. *Bifurcation plots for the $N = 3$ case of dynamics* (2.2), *constant edge weights $b = 0.2$ and mutation matrix* (Q2). *The x-axis in each plot is the mutation strength μ, blue and red curves are stable and unstable equilibria, respectively, and the magenta curves are stable limit cycles. The three-node graphs in each subplot have adjacency matrix B with self-cycles (not shown) at each node.*
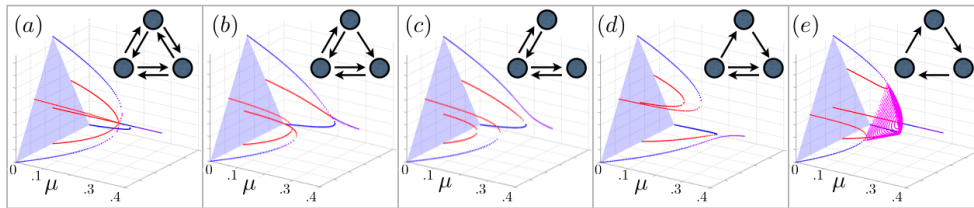
Note that for $\mu = 0$ the only stable equilibria for the replicator-mutator dynamics with payoffs (2.1) are the three (dominant) pure strategy equilibria at the corners of the triangle simplex. In all the subplots in Figures 3.3 and 3.4, bifurcations yield a unique mixed strategy equilibrium in the interior of the simplex, for increasing μ. The transition from the dominant equilibria to the mixed equilibrium for increasing μ depends strongly on the topology of the payoff graph B under consideration. In the case of all-to-all interconnections in Figure 3.3(a) and 3.4(a), the mixed equilibrium

---

[1]Equilibria and nullclines are solved using the MATLAB® symbolic toolbox.

$\boldsymbol{x_{mix,3}} = \frac{1}{3}\mathbf{1}_3$ changes stability via an $\mathcal{S}_3$-symmetric transcritical bifurcation (see [3] for details). The bifurcation plots for graphs in Figures 3.3(b)-(d) and 3.4(b)-(d) each have a stable branch of equilibria for all μ. They also have two other stable and four unstable equilibria at $\mu = 0$ which disappear in saddle-node bifurcations as μ increases. We note that these bifurcations are qualitatively representative of bifurcations generally observed in small perturbations of the structurally unstable symmetric all-to-all case. The bifurcations in Figures 3.3(b)-(d) and 3.4(b)-(d) are also comparable to the saddle-node bifurcations for the $N = 2$ dynamics studied in [11].

The bifurcation plots in Figures 3.3(e) and 3.4(e) correspond to a directed cycle interconnection among nodes in the payoff graph. The equilibrium $\boldsymbol{x_{mix,3}}$ exists for all values of $\mu \in [0,1]$. In Figure 3.3(e), three symmetric saddle-node bifurcations occur at $\mu = \mu_{C1}$ and stable limit cycles appear about $\boldsymbol{x_{mix,3}}$. These are followed by a Hopf bifurcation at $\mu = \mu_{C2}$, where $\boldsymbol{x_{mix,3}}$ changes stability from an unstable to a stable focus and the limit cycles disappear. Figure 3.5 shows phase portraits of the dynamics for various choices of μ, illustrating the Hopf bifurcation.

(a) $\mu = 0$

(b) $\mu = 0.1 < \mu_{C1}$

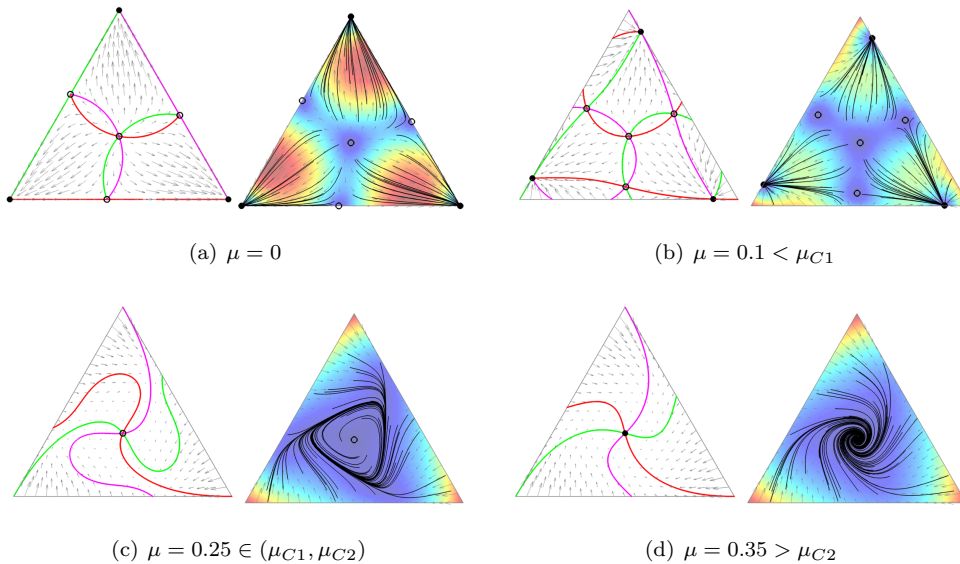(c) $\mu = 0.25 \in (\mu_{C1}, \mu_{C2})$

(d) $\mu = 0.35 > \mu_{C2}$

FIG. 3.5. *Phase portraits for dynamics* (2.2) *and with directed cycle topology as in Figure 3.3(e) and mutation matrix (Q1). The figure on the left of each of the four sub-figures shows nullclines (red, green and magenta), vector field (grey arrows) and equilibria (filled circles are stable, unfilled circles are unstable). The figure on the right of each of the four sub-figures shows sample trajectories for randomly chosen initial conditions. The color scale indicates the magnitude of the flow (vector field) with hot colors corresponding to fast flow. $b = 0.2$ for this set of plots which gives $\mu_{C1} = 0.212$ and $\mu_{C2} = 0.3$. See accompanying animation phasecyc.mpg [3.1MB].*

In [22] we proved that stable limit cycles of the dynamics exist in a wide region of parameter space for circulant payoff matrices B, for which the directed cycle topology in Figure 3.3(e) is a special case. Here we state two of the main results from [22] that provide necessary and sufficient conditions for the existence of stable limit cycles for

(2.2) with circulant payoff matrix given by

$$B := B_{C,3} = \text{Circulant}(1, \alpha, \beta) = \begin{bmatrix} 1 & \alpha & \beta \\ \beta & 1 & \alpha \\ \alpha & \beta & 1 \end{bmatrix}, \ \{\alpha, \beta\} \in [0, 1) \text{ and } \alpha + \beta > 0.$$

Lemma 3.1 provides necessary conditions for the existence of limit cycles for (2.2) with $N = 3$ and payoff matrix $B_{C,3}$. Corollary 3.2 provides sufficient conditions for Hopf bifurcations and stable limit cycles and is a special case of the more general result in Theorem 4.5 to follow in §4.

LEMMA 3.1. *The dynamics* (2.2) *with payoff matrix $B_{C,3}$ have no closed orbits in the simplex Δ_2 for*

$$\mu > \frac{(2 - \alpha - \beta)(\alpha + \beta)}{6(\alpha + \beta + \alpha\beta)} =: \mu_{01} \text{ for mutation (Q1), and}$$

$$\mu > \frac{2(2 - \alpha - \beta)}{3(4 + \alpha + \beta)} =: \mu_{02} \text{ for mutation (Q2).}$$

Proof. Follows from a straightforward application of Bendixson's Criterion; refer to [22] for details.   ☐

COROLLARY 3.2. *Equilibrium $\boldsymbol{x_{mix,3}}$ of the dynamics* (2.2) *with $N = 3$ strategies, payoff matrix $B_{C,3}$, mutation matrix (Qi) (i = 1, 2) and bifurcation parameter μ, undergoes a supercritical Hopf bifurcation at $\mu = \mu_{0i}$ leading to stable limit cycles for $\mu < \mu_{0i}$ if $\alpha \neq \beta$ and additionally if $2\alpha + 2\beta + 5\alpha\beta + \alpha^2 + \beta^2 \neq 2$ for mutation matrix* (Q1).

Proof. The proof relies on satisfying the conditions of the Hopf Bifurcation Theorem 4.3. This is shown for $N \geq 3$ in Theorem 4.5. For $N = 3$, the first Lyapunov coefficient is given by $\ell_1(\alpha, \beta) = \frac{3(\alpha + \beta - 2)}{\omega_{0i}}$, where,

$$\omega_{0i} = |\tilde{\omega}_i|, \ \ \tilde{\omega}_i = \begin{cases} \frac{(\alpha - \beta)(\alpha^2 + \beta^2 + 2\alpha + 2\beta + 5\alpha\beta - 2)}{6\sqrt{3}(\alpha + \beta + \alpha\beta)} & i = 1 \\ \frac{(\alpha - \beta)(1 + \alpha + \beta)}{\sqrt{3}(4 + \alpha + \beta)} & i = 2. \end{cases}$$

This follows from the calculation of ℓ_1 in Lemma 4.6. Supercriticality follows from $\omega_{0i} \neq 0 \implies \ell_1 < 0$.   ☐

Figure 3.3(e) shows limit cycles for the specific case of $B_{C,3}$ with $\alpha = b$ and $\beta = 0$. Figure 3.6 shows three more limit cycle bifurcation plots for non-zero α and β and mutation matrix (Q1). Interestingly, for the parameter values selected in Figure 3.6(b) stable limit cycles coexist with multiple stable equilibria. This coexistence of stable equilibria and stable limit cycles implies that different initial conditions can yield qualitatively distinct limiting behavior even with fixed parameters for the dynamics (i.e., without bifurcations).

4. Hopf Bifurcation Analysis. In §3 we looked at Hopf bifurcations for the replicator-mutator dynamics (2.2) with $N = 3$ strategies and circulant payoff matrix $B_{C,3}$. While the focus on three strategies was convenient for visualization, the simulations in Figure 3.2 indicate that the dynamics have stable limit cycles in higher dimensions as well ($N \geq 4$). In this section we show that this is indeed the case by proving two main results. Theorem 4.5 shows that the dynamics undergo multiple
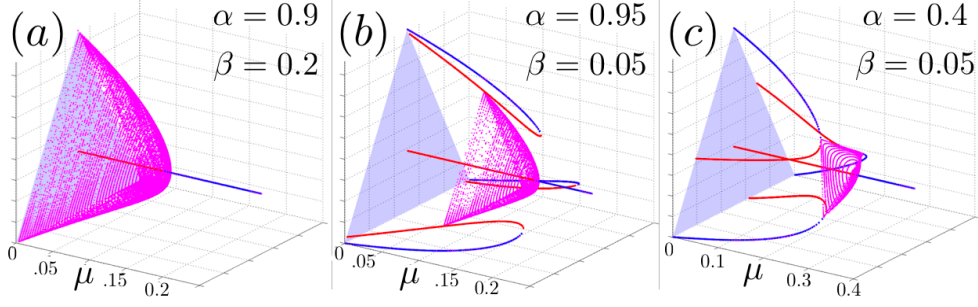
FIG. 3.6. *Bifurcation plots for the dynamics* (2.2), *payoff matrix $B_{C,3}$ and parameters α and β as shown. The existence of Hopf bifurcations and stable limit cycles for the set of parameter choices follows from Corollary 3.2. Note the coexistence of stable equilibria with stable limit cycles in panel (b).*

Hopf bifurcations at distinct bifurcation points, and Lemma 4.6 provides analytical conditions for the stability of the limit cycles arising from these Hopf bifurcations.

We focus on the dynamics with circulant payoff matrix $B_{C,N} \in \mathbb{R}^{N \times N}, N \geq 3$ given by

$$B_{C,N} := \text{Circulant}\,(1, \alpha, 0, \cdots, 0, \beta)\,, \{\alpha, \beta\} \in [0,1) \text{ and } \alpha + \beta > 0, \qquad (4.1)$$

and mutation matrices (Q1) and (Q2). The directed graph induced by the payoff matrix $B_{C,N}$ is illustrated in Figure 4.1.
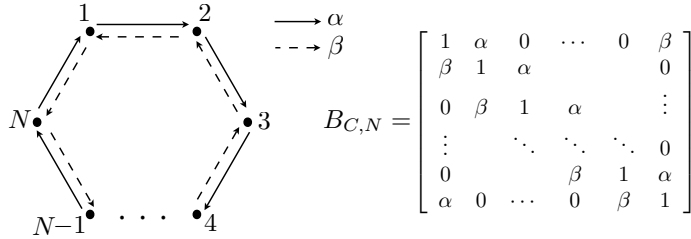

FIG. 4.1. *Graph topology corresponding to the two-parameter payoff matrix $B_{C,N}$ from* (4.1).

We have chosen to study the circulant two-parameter payoff structure $B_{C,N}$ both for purposes of tractability and to gain important insights regarding Hopf bifurcations of the dynamics in N dimensions. In particular, we show the existence of multiple Hopf bifurcations as several distinct pairs of eigenvalues cross the imaginary axis with increasing mutation parameter μ. Further, the criticality of the bifurcations, and correspondingly the existence of stable limit cycles, depends on the choice of parameters α and β, unlike the $N = 3$ case where all existing bifurcations are supercritical. The analysis also shows that the choice of the mutation matrix (Q1) and (Q2) plays an important role in determining the existence and criticality of the Hopf bifurcations.

For payoff matrix $B_{C,N}$, the equilibrium $\boldsymbol{x_{mix,N}} = \frac{1}{N}\boldsymbol{1}_N = \left[\frac{1}{N} \cdots \frac{1}{N}\right]^T \in \mathbb{R}^N$ undergoes the Hopf bifurcations. Lemma 4.1 shows that $\boldsymbol{x_{mix,N}}$ is always an equilibrium of (2.2) for circulant B.

LEMMA 4.1. *If the payoff matrix B is circulant, then $\boldsymbol{x_{mix,N}}$ is an equilibrium of the replicator-mutator dynamics* (2.2).

Proof. Suppose B is circulant. Then $\mathbf{1}$ is an eigenvector of B with eigenvalue $r_B = \sum_{j=1}^{N} b_{1j}$, i.e., $B\mathbf{1} = r_B\mathbf{1}$. Matrix Q is also circulant by construction from (Q1) and (Q2). This means that $\sum_{j=1}^{N} q_{ji} = \sum_{j=1}^{N} q_{ij} = 1$. Let $\boldsymbol{x} = \boldsymbol{x_{mix,N}}$. Then $\boldsymbol{f} = B\boldsymbol{x_{mix,N}} = \frac{1}{N}B\mathbf{1} = \frac{r_B}{N}\mathbf{1}$. From (2.2),

$$\dot{x}_i\Big|_{\boldsymbol{x_{mix,N}}} = \frac{1}{N}\sum_{j=1}^{N} f_j\left(q_{ji} - \frac{1}{N}\right) = \frac{r_B}{N^2}\sum_{j=1}^{N} q_{ji} - \frac{r_B}{N^2} = 0,$$

and $\boldsymbol{x_{mix,N}}$ is an equilibrium. $\square$

To proceed with the analysis, we start by calculating $D_{\boldsymbol{x}}\boldsymbol{g}\big|_{\boldsymbol{x_{mix,N}}}$, the Jacobian matrix of the dynamics evaluated at the equilibrium point $\boldsymbol{x_{mix,N}}$. We then prove conditions for the existence of $\lfloor\frac{N-1}{2}\rfloor$ pairs of complex conjugate eigenvalues of the Jacobian. We prove that each of these pairs of complex eigenvalues has distinct real part and hence each pair crosses the imaginary axis at different values of the bifurcation parameter μ. We show that each such crossing satisfies the conditions of the Hopf Bifurcation Theorem 4.3. We then derive an analytic expression for the sign of the first Lyapunov coefficient ℓ_1 for each of the Hopf bifurcations in terms of the payoff parameters α and β, the eigenvalues of the mutation matrix Q, the Jacobian $D_{\boldsymbol{x}}\boldsymbol{g}\big|_{\boldsymbol{x_{mix,N}}}$, and the particular critical μ at which the bifurcation occurs.

4.1. Hopf Bifurcation Calculation. By Lemma 4.1, $\boldsymbol{x_{mix,N}}$ is an equilibrium for the replicator-mutator dynamics (2.2) with circulant payoff $B_{C,N}$. The (i,j) entry of the Jacobian $D_{\boldsymbol{x}}\boldsymbol{g}\big|_{\boldsymbol{x_{mix,N}}}$, denoted $\left[D_{\boldsymbol{x}}\boldsymbol{g}\big|_{\boldsymbol{x_{mix,N}}}\right]_{ij}$, is given by

$$\frac{1}{N}\left[(2+\alpha+\beta)\,q_{ji} + \alpha q_{j-1,i} + \beta q_{j+1,i} - \left(\frac{2}{N}+\delta_{ij}\right)(1+\alpha+\beta)\right], \tag{4.2}$$

where δ_{ij} is the Kronecker delta and the indices i,j are denoted modulo N, i.e. $1 \equiv N+1, 0 \equiv N$, etc. For circulant fitness B, the Jacobian $D_{\boldsymbol{x}}\boldsymbol{g}\big|_{\boldsymbol{x_{mix,N}}}$ is also circulant.

Let $\omega_N = \cos\left(\frac{2\pi}{N}\right) + \mathbf{i}\sin\left(\frac{2\pi}{N}\right)$ be a complex, primitive N^{th} root of unity. Let $\omega_{N,k} = \omega_N^k = \cos\left(\frac{2\pi}{N}k\right) + \mathbf{i}\sin\left(\frac{2\pi}{N}k\right)$ for any integer k. For a circulant matrix $M = [m_{ij}] \in \mathbb{R}^{N\times N}$, let

$$\lambda_k(M) = \sum_{j=1}^{N} m_{1j}\,\omega_{N,k}^{j-1}. \tag{4.3}$$

Then, the N eigenvalues of M are $\{\lambda_k(M), \lambda_{k+1}(M), \cdots, \lambda_{N+k-1}(M)\}$ for any k [8]. Lemma 4.2 provides necessary and sufficient conditions for the existence of complex eigenvalues for the Jacobian $D_{\boldsymbol{x}}\boldsymbol{g}\big|_{\boldsymbol{x_{mix,N}}}$.

LEMMA 4.2. *The Jacobian $D_{\boldsymbol{x}}\boldsymbol{g}\big|_{\boldsymbol{x_{mix,N}}}$ has $\lfloor\frac{N-1}{2}\rfloor$ pairs of complex conjugate eigenvalues if and only if $\alpha \neq \beta$ and*

$$\mu \neq \frac{\alpha+\beta}{2(1+\alpha+\beta)} \text{ for mutation (Q1), or, } \mu \neq \frac{N-1}{N} \text{ for mutation (Q2).}$$

Proof. The proof relies on the cyclic properties of complex roots of unity. Details are in Appendix A.   □

Note that if the conditions in Lemma 4.2 are not satisfied (neither for the mutation (Q1) nor for the mutation (Q2)), then the eigenvalues of the Jacobian are strictly real. When the conditions are satisfied, $\omega_{N,k}$ is complex if and only if $\lambda_k\left(D_{\boldsymbol{x}}\boldsymbol{g}|_{\boldsymbol{x}_{mix,N}}\right)$ is complex. There are $\left\lfloor\frac{N-1}{2}\right\rfloor$ complex conjugate pairs among the $\omega_{N,k}$ for $k = 1, \cdots, N$. For $N = 3$, the one complex pair is associated with the unique Hopf bifurcation point as seen in Figures 3.3(e), 3.4(e) and 3.6.

For notational consistency, we state the Hopf bifurcation theorem (Theorem 3.4.2 from [4]) which will be used to prove the existence of stable limit cycles for the dynamics.

THEOREM 4.3. *Suppose that the system* $\dot{\boldsymbol{x}} = \boldsymbol{f}(\boldsymbol{x}, \mu)$, $\boldsymbol{x} \in \mathbb{R}^N$, $\mu \in \mathbb{R}$, *has an equilibrium* $(\boldsymbol{x_0}, \mu_0)$ *and the following properties are satisfied:*

- *(H1) The Jacobian* $D_x\boldsymbol{f}|_{(\boldsymbol{x_0},\mu_0)}$ *has a simple pair of pure imaginary eigenvalues* $\lambda(\mu_0)$ *and* $\overline{\lambda(\mu_0)}$ *and no other eigenvalues with zero real parts,*
- *(H2)* $\frac{d}{d\mu}\left(Re\ \lambda(\mu)\right)\Big|_{(\mu=\mu_0)} \neq 0.$

Then the dynamics undergo a Hopf bifurcation at $(\boldsymbol{x_0}, \mu_0)$ *resulting in periodic solutions. The stability of the periodic solutions is given by the sign of the first Lyapunov coefficient of the dynamics* $\ell_1|_{(\boldsymbol{x_0},\mu_0)}$. *If* $\ell_1 < 0$ *then these solutions are stable limit cycles and the Hopf bifurcation is supercritical, while if* $\ell_1 > 0$ *the periodic solutions are repelling.* Details of the calculation of the Lyapunov coefficient ℓ_1 are provided in Appendix B.

To prove the existence of Hopf bifurcations we need to show that conditions (H1) and (H2) of Theorem 4.3 are satisfied. We begin by calculating critical values of the bifurcation parameter μ corresponding to pairs of eigenvalues crossing the imaginary axis. Since mutation matrices (Q1) and (Q2) have entries that are linear in μ, the entries of the Jacobian $D_{\boldsymbol{x}}\boldsymbol{g}|_{\boldsymbol{x}_{mix,N}}$ are also all linear in μ. In order to simplify the notation, we set

$$\left[D_{\boldsymbol{x}}\boldsymbol{g}|_{\boldsymbol{x}_{mix,N}}\right]_{1j} = \gamma_j + \mu\eta_j,\ j = 1, \cdots, N, \tag{4.4}$$

where both γ_j and η_j are independent of μ. Using this notation, we compute the bifurcation points for the dynamics in Lemma 4.4.

LEMMA 4.4. *The pair of complex conjugate eigenvalues* λ_r, λ_{N-r} *of the Jacobian* $D_{\boldsymbol{x}}\boldsymbol{g}|_{\boldsymbol{x}_{mix,N}}$, *for each* $r = 1, \cdots, \left\lfloor\frac{N-1}{2}\right\rfloor$, *is purely imaginary if and only if*

$$\mu = -\left[\sum_{j=1}^{N}\gamma_j\cos\left(\frac{2\pi}{N}(j-1)r\right)\right]\left[\sum_{j=1}^{N}\eta_j\cos\left(\frac{2\pi}{N}(j-1)r\right)\right]^{-1} =: \mu_{0,r}, \tag{4.5}$$

and $\mu_{0,r}$ *satisfies the conditions of Lemma 4.2. Further, the bifurcation points* $\mu_{0,r}$ *are distinct, i.e.* $\mu_{0,k} \neq \mu_{0,l}$ *when* $k \neq l$.

Proof. The proof is in Appendix C.   □

From Lemma 4.4, a unique pair of eigenvalues of $D_{\boldsymbol{x}}\boldsymbol{g}|_{(\boldsymbol{x}_{mix,N},\mu_{0,r})}$ is purely imaginary at each $\mu_{0,r}$; this implies condition (H1). Lemma 4.4 also implies that $\frac{d}{d\mu}\text{Re}\left(\lambda_r\right) = \sum_{j=1}^{N}\eta_j\cos\left(\frac{2\pi}{N}(j-1)r\right) \neq 0$, which is condition (H2). We can now collect these results and state our main theorem.

THEOREM 4.5. *The equilibrium point $\boldsymbol{x_{mix,N}}$ with payoff matrix $B_{C,N}$ undergoes $\lfloor \frac{N-1}{2} \rfloor$ Hopf bifurcations, with the rth $\left(r = 1, \cdots, \lfloor \frac{N-1}{2} \rfloor\right)$ of such bifurcations located at $\mu_{0,r}$ given by (4.5), if $\alpha \neq \beta$ and*

$$\mu_{0,r} \neq \frac{\alpha + \beta}{2\left(1 + \alpha + \beta\right)} \ \text{ for mutation (Q1), or, } \mu_{0,r} \neq \frac{N-1}{N} \ \text{ for mutation (Q2).}$$

REMARK 1. *Equation (4.5) gives an analytic expression for $\mu_{0,r}$ corresponding to a unique pair of purely imaginary eigenvalues of the Jacobian. However, not all values of $\mu_{0,r}$ are feasible. That is, there might be pairs $(\alpha, \beta) \in [0,1) \times [0,1)$ that yield bifurcation points $\mu_{0,r}$ outside the feasible parameter range $0 \leq \mu_{0,r} \leq 1$ of our model.*

4.2. Criticality of the Hopf Bifurcation. In Theorem 4.5 we proved conditions for the existence of Hopf bifurcations for the replicator-mutator dynamics with payoff $B_{C,N}$. In this section we study the criticality of the bifurcations (and correspondingly the existence of stable limit cycles for the dynamics) by computing an analytical expression for the first Lyapunov coefficient $\ell_1|_{(\boldsymbol{x_{mix,N}},\mu_{0,r})}$ in Lemma 4.6.

LEMMA 4.6. *Let $A_0 = D_{\boldsymbol{x}}\boldsymbol{g}|_{(\boldsymbol{x_{mix,N}},\mu_{0,r})}$. Then A_0 has a pair of purely imaginary eigenvalues $\lambda_r(A_0) = \mathbf{i}\,\hat{\omega}$ and $\lambda_{N-r}(A_0) = -\mathbf{i}\,\hat{\omega}$, where $\hat{\omega} \in \mathbb{R}$ is calculated from (4.3). Define $t = r\,\mathrm{sign}\,(\hat{\omega})$ and $\omega_0 = |\hat{\omega}|$. The first Lyapunov coefficient of the dynamics (2.2) with payoff $B_{C,N}$ evaluated at the fixed point $\boldsymbol{x_{mix,N}}$ and bifurcation point $\mu_{0,r}$ is given by*

$$\ell_1|_{(\boldsymbol{x_{mix,N}},\mu_{0,r})} = \frac{1}{2\omega_0}\mathrm{Re}\,(T_1 + T_2)\,, \ \text{where,}$$

$$T_1 = -2N\left[2 + (\alpha+\beta)(\omega_N^t + \omega_N^{-t})\right] \ \text{ and}$$

$$T_2 = \frac{2\lambda_t(Q^T)\,\lambda_{2t}(Q^T)}{2\,\mathbf{i}\,\omega_0 - \lambda_{2t}(A_0)}\left(1 + \alpha\omega_N^t + \beta\omega_N^{-t}\right)\left[2 + \left(1 + \omega_N^{3t}\right)\left(\beta\omega_N^{-2t} + \alpha\omega_N^{-t}\right)\right].$$

Proof. The function $\lambda_k(M)$ is defined for general integer k and square matrix M in (4.3). We exploit the circulant structure of the dynamics to obtain this analytical result. Details of the calculation are in Appendix D. □

Lemma 4.6 allows us to study the criticality of the Hopf bifurcations at each of the bifurcation points $\mu_{0,r}$ as a function of the parameters $(\alpha, \beta) \in [0,1) \times [0,1)$. In Figure 4.2 we plot regions of positive and negative ℓ_1 as a function of α and β. For each of the subplots in Figure 4.2, black denotes negative l_1 (supercritical Hopf bifurcation, stable limit cycles) and white denotes positive l_1 (subcritical Hopf bifurcation, repelling periodic solutions). Gray denotes the unfeasibility region for $\mu_{0,r}$ (either $\mu_{0,r} < 0$ or $\mu_{0,r} > 1$, see Remark 1). The red curves correspond to critical points $\mu_{0,r}$ that do not satisfy the conditions of Lemma 4.2.

Figure 4.2 illustrates the effect of the number of strategies N and payoff parameters α and β on the existence and criticality of Hopf bifurcations for the dynamics. Several different cases exist. For example, there are cases corresponding to a supercritical bifurcation throughout $(\alpha, \beta) \in [0,1) \times [0,1)$ (as when $N = 3$), and cases for which the bifurcation is subcritical on a subset of the parameter space (as when $N = 4$ with mutation matrix (Q2)). The regions corresponding to infeasible critical points ($\mu_{0,r}$ outside the range $[0,1]$) can be connected as when $N = 8$, $r = 3$, or disconnected, as when $N = 6$, $r = 1$ with mutation matrix (Q1). Some cases are illustrated in §4.3.
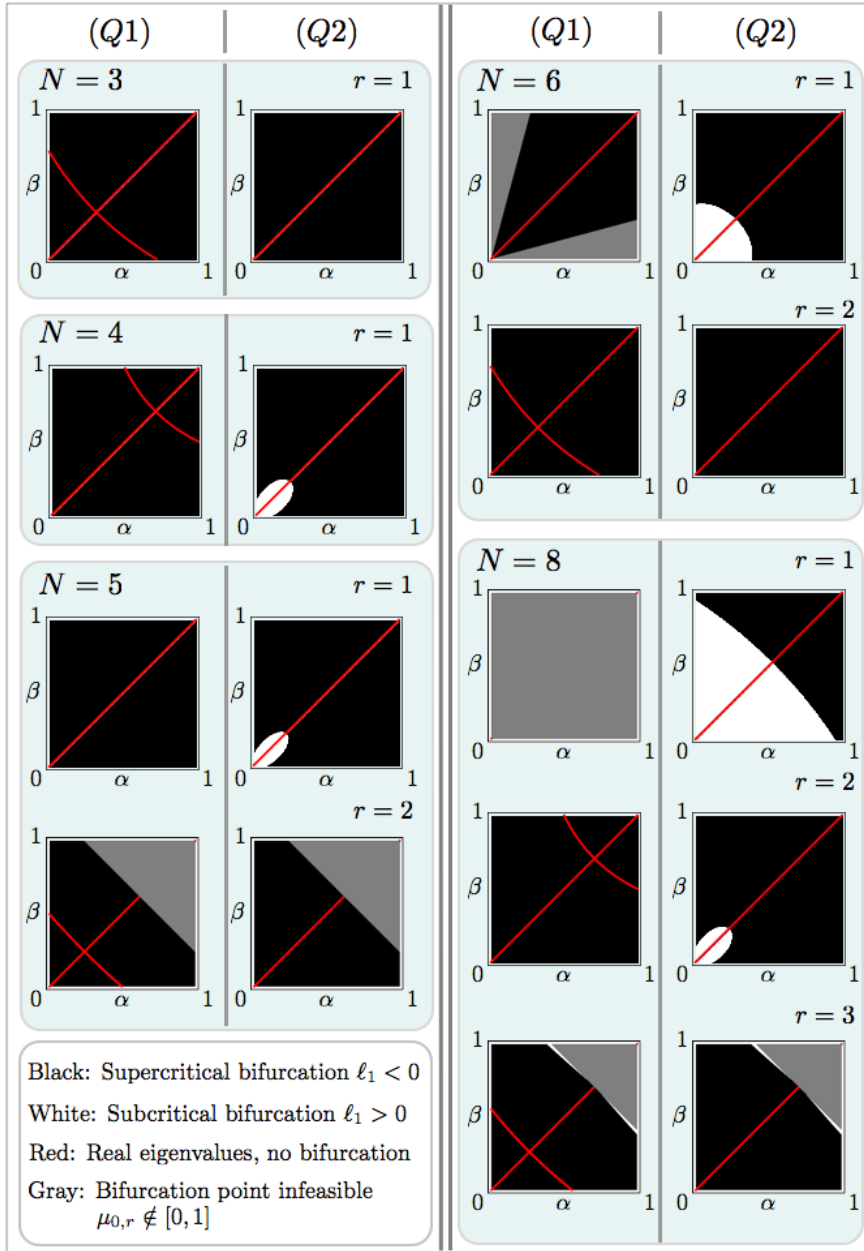
Fig. 4.2. *Criticality of the Hopf bifurcations as a function of parameters α and β.*

4.3. Illustrations of Hopf Bifurcations. The existence and criticality of Hopf bifurcations computed in Lemma 4.4 and Theorem 4.5 vary as a function of parameters α and β in ways that may not be immediately obvious. In this subsection, we explore the parameter dependence of the Hopf bifurcations using a set of selected simulations to help illustrate this variation.

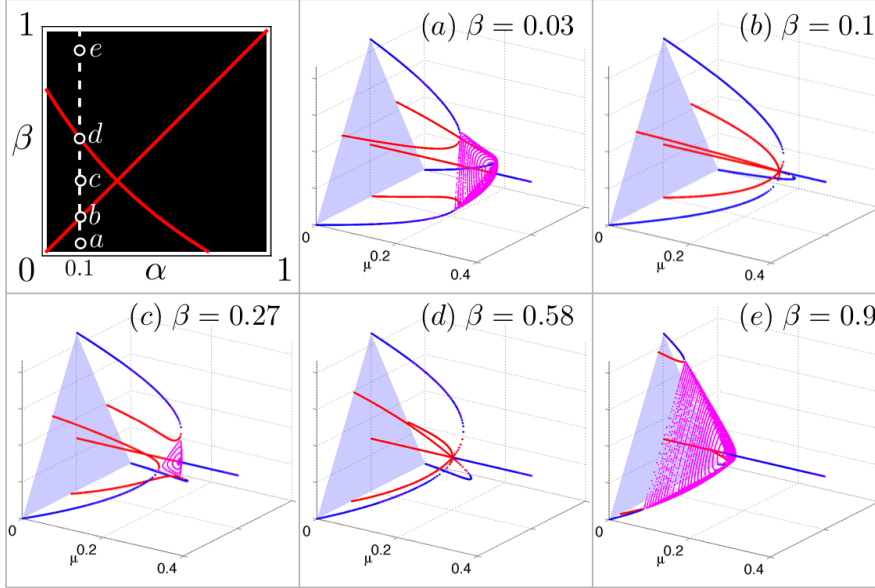Figure 4.3 (and accompanying animation slice.mpg [1.8MB]) shows bifurcation

FIG. 4.3. *Effect of parameters α and β on bifurcations. Subplots labeled (a)–(e) are bifurcation plots for the dynamics with $N = 3$ strategies, mutation matrix (Q1), $\alpha = 0.1$ and β as shown. The top left subplot shows the criticality and existence of the Hopf bifurcations (taken from Figure 4.2: $N = 3$, (Q1)) with parameters corresponding to subplots (a)–(e) marked. The amplitude of oscillations gets smaller as $\beta \to \alpha$ (approaching subplot (b)) and as $2\alpha + 2\beta + 5\alpha\beta + \alpha^2 + \beta^2 \to 2$ (approaching subplot (d)). See accompanying animation slice.mpg [1.8MB].*
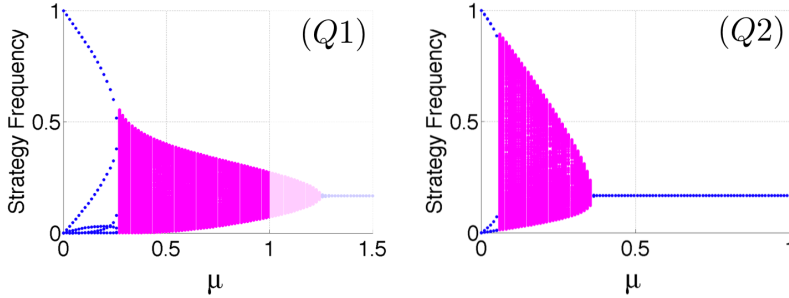

FIG. 4.4. *Bifurcation plots for the dynamics with $N = 6$ strategies, parameters $\alpha = 0.8$, $\beta = 0.05$, and mutation matrix as indicated on each subplot. In the case of the left subplot with mutation matrix (Q1), the Hopf bifurcation point $\mu_{0,1} = 1.24$ lies outside the feasible range $\mu \in [0, 1]$.*

plots for the dynamics with $N = 3$ and mutation matrix (Q1). Parameter α is set to 0.1 and β is varied between 0 and 1. Looking at the corresponding criticality plot in Figure 4.3 (reproduced from Figure 4.2), we expect that the bifurcation is supercritical for all β except at two points labeled (b) and (d). These are precisely the points that violate the conditions of Lemma 4.2 and Theorem 4.5. i.e., at (b), $\alpha = \beta = 0.1$ and at (d), $\mu_{0,1} = \frac{\alpha+\beta}{2(1+\alpha+\beta)}$ for $\alpha = 0.1$ and $\beta = 0.58$. As a result, the bifurcation plots show the existence of stable limit cycles for all values of β along the line $\alpha = 0.1$, except at the points (b) and (d). Stable limit cycles are apparent in Figures 4.3(a), 4.3(c) and 4.3(e), but not in Figures 4.3(b) and 4.3(d). The payoff topology corresponding to the parameters in Figure 4.3(b) is fully symmetric, with a

bifurcation plot analogous to Figure 3.3(a).

Figure 4.4 shows the bifurcation plots for the dynamics with $N = 6$, $\alpha = 0.8$, $\beta = 0.05$, and mutation matrices (Q1) and (Q2). The corresponding criticality plots in Figure 4.2 show that the supercritical Hopf bifurcation point $\mu_{0,1}$ lies outside the feasible range $\mu \in [0, 1]$ for (Q1) and inside the feasible range for (Q2), for the chosen parameters. This is illustrated in Figure 4.4; the left plot shows a Hopf bifurcation at $\mu = 1.249$ while the right plot shows a Hopf bifurcation at $\mu = 0.363$. The left plot in Figure 4.4 also illustrates that infeasible supercritical bifurcation points can yield stable limit cycles within the range of feasible μ.

5. $N \geq 4$ One Parameter Circulant. In §4 we focused on a particular two-parameter circulant payoff structure given by (4.1) and illustrated in Figure 4.1. In this section we leverage the results from §4 to study the dynamics corresponding to a class of circulant payoff structures with each node having a single outgoing edge. For simplicity of presentation, we consider only mutation matrix (Q1) in this section. We show that for a particular set of topologies in this class, the dynamics exhibit multiple simultaneous Hopf bifurcations about distinct fixed points. The analysis in this section points to the fact that the dynamics with payoff graphs having multiple embedded cycles can have multiple distinct stable limit cycle attractors; we explore these multi-cycle dynamics more generally in §6.
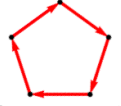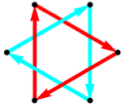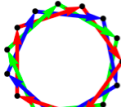

	Case 1 $d = 1$	Case 2	Case 3 $d = N/2$
$N = 5$	$k = 1, 2, 3, 4$		
$N = 6$	$k = 1, 5$	$d = 2; \quad k = 2, 4$	$k = 3$
$N = 15$	$k = 1, 2, 4, 7$ $8, 11, 13, 14$	$d = 3$ $k = 3, 6, 9, 12$ $\quad$ $d = 5$ $k = 5, 10$	

FIG. 5.1. *Graph topologies corresponding to circulant payoff matrix $B_{N,k}$ from (5.1) for $N = 5, 6, 15$. Three cases are shown, Case 1 corresponds to simple cycles, Case 2 to multiple cycles, and Case 3 to connected pairs of vertices (only exists for N even). Note that multiple values of k can yield the same graph topology modulo a vertex relabeling; non-isomorphic topologies have distinct d.*

Consider the dynamics (2.2) where the payoff matrix B is given by

$$B := B_{N,k} = \text{Circulant}\,(1, a_1, \cdots, a_{N-1})\,, \text{ with } a_k = \alpha \text{ and } a_s = 0 \text{ for } s \neq k. \quad (5.1)$$

Let $\gcd(a, b)$ denote the greatest common divisor of a and b. Two graphs with payoff matrices B_{N,k_1} and B_{N,k_2} are isomorphic if and only if $\gcd(N, k_1)=\gcd(N, k_2)$. Hence, among the payoff matrices $B_{N,k}$, the set of matrices $B_{N,d}$ where d belongs to the set

of proper divisors of N, corresponds to a set of non-isomorphic graph topologies. We split the set of graph topologies with payoff $B_{N,d}$ (d a proper divisor of N) into three distinct cases as described below:

(1) $d = 1$, the graph is a directed cycle containing all vertices
(2) $1 < d < N/2$, the graph consists of d disjoint cycles, each of length N/d
(3) $d = N/2$, the graph consists of $N/2$ disjoint pairs of connected vertices. This case exists only for N even.

Figure 5.1 illustrates the three cases of graph topologies for $N = 5,\ 6,$ and 15.

In addition to $\boldsymbol{x_{mix,N}}$, the dynamics with payoff matrix $B_{N,d}$ and mutation matrix (Q1) have d equilibria denoted $\boldsymbol{x_{j,d,N}}$ and given by

$$\boldsymbol{x_{j,d,N}} = \left[\ \boldsymbol{0}^T_{j-1}\quad \tfrac{d}{N}\quad \boldsymbol{0}^T_{d-j}\ \middle|\ \cdots\ \middle|\ \boldsymbol{0}^T_{j-1}\quad \tfrac{d}{N}\quad \boldsymbol{0}^T_{d-j}\ \right]^T \in \mathbb{R}^N,\ j = 1, \cdots, d. \quad (5.2)$$

In Case 1, $d = 1$, and correspondingly $j = 1$, and $\boldsymbol{x_{1,1,N}} = \boldsymbol{x_{mix,N}}$. For a given N and $d \neq 1$, the d equilibria $\boldsymbol{x_{j,d,N}}$ are cyclically and symmetrically spaced around $\boldsymbol{x_{mix,N}}$. Case 1 is studied in detail in §4 and obtained by setting $\beta = 0$ (a simple one-parameter cycle). For the topology with pairs of connected nodes in Case 3, the Jacobian of (2.2) evaluated at the equilibrium $\boldsymbol{x_{mix,N}}$, or also at any of the equilibria $\boldsymbol{x_{j,N/2,N}}$, is real and symmetric and therefore has only real eigenvalues. Thus the system cannot have Hopf bifurcations for these equilibria in this case. We now focus on Case 2 and study the dynamics with payoff topologies comprising multiple cycles.

5.1. Case 2 Analysis. We begin the analysis of the dynamics with multi-cycle graph topologies by first looking at the case $N = 6$, $d = 2$ (payoff $B_{6,2}$), before generalizing to higher dimensions. The two disjoint cycles in the graph corresponding to $B_{6,2}$ suggest that the behavior of the system might be similar to that observed for the $N = 3$ cycles in §3. Indeed, simulations of the dynamics shown in Figure 5.2 suggest the existence of two stable limit cycle attractors, each dominated exclusively by three strategies, corresponding to the connected nodes of the graph. Further, simulations of the phase space for 50 different randomly selected initial conditions, as in Figure 5.2(b), indicate that the two limit cycles are the only stable attractors for the dynamics for an appropriate range of bifurcation parameter μ.

The linearization of the system at equilibrium $\boldsymbol{x_{mix,6}}$ violates condition (H1) of Theorem 4.3 (i.e., complex eigenvalues of the Jacobian have algebraic multiplicity greater than one). However the dynamics with payoff $B_{6,2}$ have two other equilibria (as in (5.2)) given by

$$\boldsymbol{x_{1,2,6}} = \left[\ 1/3\quad 0\quad 1/3\quad 0\quad 1/3\quad 0\ \right]^T,$$
$$\boldsymbol{x_{2,2,6}} = \left[\ 0\quad 1/3\quad 0\quad 1/3\quad 0\quad 1/3\ \right]^T.$$

The simulations in Figure 5.2 suggest that the dynamics undergo Hopf bifurcations at each of these equilibria. In Corollary 5.1, which follows from Corollary 3.2, we prove that this is indeed the case by showing that $\boldsymbol{x_{1,2,6}}$ and $\boldsymbol{x_{2,2,6}}$ undergo two simultaneous Hopf bifurcations at the critical point $\mu = \frac{2-\alpha}{6}$.

COROLLARY 5.1. *The system* (2.2) *with payoff matrix $B_{6,2}$ and mutation matrix* (Q1) *has equilibria $\boldsymbol{x_{1,2,6}}$ and $\boldsymbol{x_{2,2,6}}$ that undergo supercritical Hopf bifurcations at the critical point $\mu = \frac{2-\alpha}{6}$ with $\alpha \neq \sqrt{3} - 1$.*

Proof. Here we analyze the equilibrium $\boldsymbol{x_{1,2,6}}$. The analysis for $\boldsymbol{x_{2,2,6}}$ is similar.
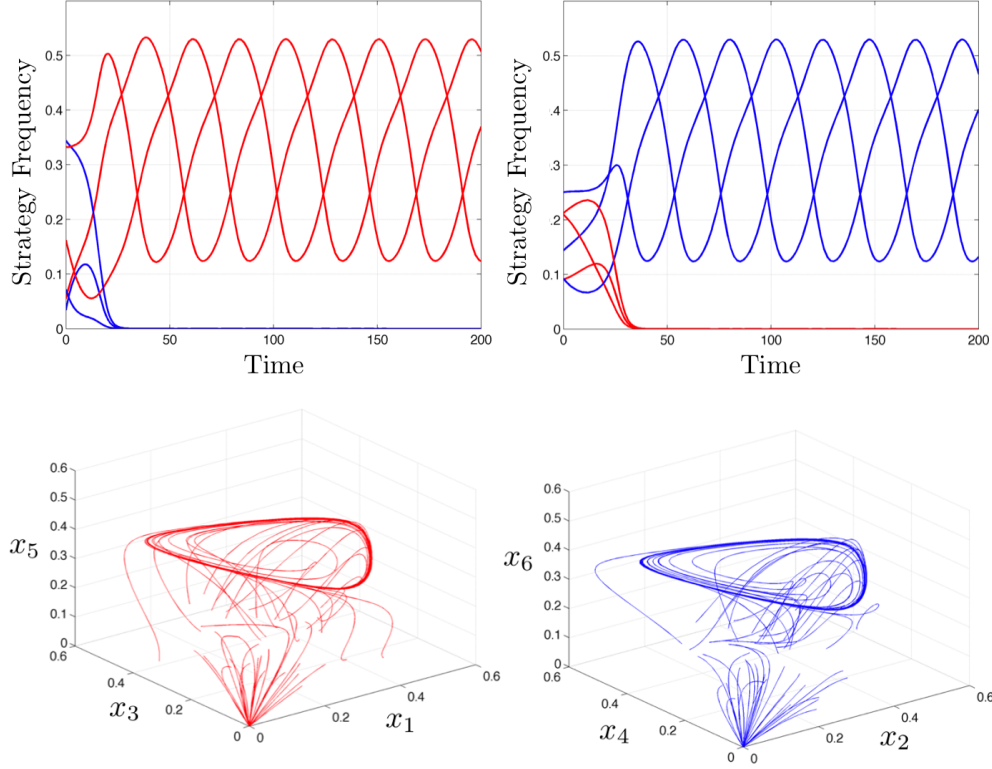
FIG. 5.2. *Simulations of the dynamics* (2.2) *for* $N = 6$, $d = 2$, *payoff matrix* $B_{6,2}$, *and* $\mu = 0.25$. *The top row of plots shows two typical trajectories of the system for two different random initial conditions. The bottom row illustrates the corresponding limit cycle attractors of the dynamics in a decoupled phase space with 50 trajectories initialized randomly. The two stable limit cycle attractors are each dominated strictly by three strategies. The red trajectories correspond to the components* x_1, x_3 *and* x_5, *and the blue trajectories correspond to* x_2, x_4 *and* x_6, *in both rows.*

The Jacobian $D_{\boldsymbol{x}}\boldsymbol{g}|_{\boldsymbol{x}_{1,2,6}}$ is given by

$$
D_{\boldsymbol{x}}\boldsymbol{g}|_{\boldsymbol{x}_{1,2,6}} = \begin{bmatrix}
\frac{1-2\alpha-6\mu}{9} & 0 & \frac{-2+\alpha-3\alpha\mu}{9} & 0 & \frac{3\alpha\mu+6\mu-2-2\alpha}{9} & 0 \\
0 & \frac{-\alpha-1}{3} & 0 & 0 & 0 & 0 \\
\frac{3\alpha\mu+6\mu-2-2\alpha}{9} & 0 & \frac{1-2\alpha-6\mu}{9} & 0 & \frac{-2+\alpha-3\alpha\mu}{9} & 0 \\
0 & 0 & 0 & \frac{-\alpha-1}{3} & 0 & 0 \\
\frac{-2+\alpha-3\alpha\mu}{9} & 0 & \frac{3\alpha\mu+6\mu-2-2\alpha}{9} & 0 & \frac{1-2\alpha-6\mu}{9} & 0 \\
0 & 0 & 0 & 0 & 0 & \frac{-\alpha-1}{3}
\end{bmatrix}.
$$

Permuting rows and columns (i.e. reindexing the nodes), this matrix can be rewritten as the block matrix $M_{6,2}$ given by

$$
M_{6,2} = \left[\begin{array}{ccc|c}
\frac{1-2\alpha-6\mu}{9} & \frac{-2+\alpha-3\alpha\mu}{9} & \frac{3\alpha\mu+6\mu-2-2\alpha}{9} & \\
\frac{3\alpha\mu+6\mu-2-2\alpha}{9} & \frac{1-2\alpha-6\mu}{9} & \frac{-2+\alpha-3\alpha\mu}{9} & 0_{3\times3} \\
\frac{-2+\alpha-3\alpha\mu}{9} & \frac{3\alpha\mu+6\mu-2-2\alpha}{9} & \frac{1-2\alpha-6\mu}{9} & \\
\hline
& 0_{3\times3} & & -\frac{1+\alpha}{3}I_{3\times3}
\end{array} \right], \quad (5.3)
$$

which has the same eigenvalues as $D_{\boldsymbol{x}}\boldsymbol{g}|_{\boldsymbol{x}_{1,2,6}}$. The upper diagonal block of $M_{6,2}$ is the

same as the Jacobian of the system (2.2) for $N = 3$, payoff $B_{C,3}$ with $\beta = 0$, mutation (Q1) and evaluated at equilibrium $\begin{bmatrix} 1/3 & 1/3 & 1/3 \end{bmatrix}^T$. The lower diagonal block is a Hurwitz matrix. Also the two blocks are decoupled, hence the eigenvalues of $M_{6,2}$ are given by the union of the sets of eigenvalues of each block. A pair of the eigenvalues crosses the imaginary axis resulting in a Hopf bifurcation for precisely the conditions given in Corollary 3.2 with $\beta = 0$ and mutation matrix (Q1) (i.e., a critical point $\mu = \frac{2-\alpha}{6}$ and complex eigenvalue condition $\alpha \neq \sqrt{3} - 1$). In Appendix E, we leverage the reindexing and decoupling (as in $M_{6,2}$) to compute the first Lyapunov coefficient for the dynamics and show that the Hopf bifurcations in this case are supercritical. □

Following the intuition developed from the analysis of the two-cycle dynamics for $N = 6$ above, and the illustrations in Figure 5.2, we now extend the analysis to general N. Just as in the $N = 6$ case, a decoupling in the Jacobian allows us to prove the existence of multiple Hopf bifurcations about the d fixed points $\boldsymbol{x_{j,d,N}}$. The (m, n) entry for the Jacobian of the system (2.2) with payoff $B_{N,d}$ and mutation matrix (Q1) is given by

$$
[D_{\boldsymbol{x}}\boldsymbol{g}]_{mn} = (2x_n + \alpha\, x_{n+d})\, q_{nm} + \alpha x_{n-d} q_{n-d,m} - x_m\, [2x_n + \alpha\, (x_{n-d} + x_{n+d})]
$$
$$
- \left(\sum_{k=1}^{N} x_k^2 + \alpha \sum_{k=1}^{N} x_k x_{k+d} \right) \delta_{mn}. \tag{5.4}
$$

Evaluating the Jacobian from (5.4) at the equilibrium $\boldsymbol{x_{j,d,N}}$, and rearranging its rows and columns analogous to (5.3), we obtain the matrix

$$
M_{N,d} = \left[\begin{array}{c|c} A_{N_1 \times N_1} & 0_{N_2 \times N_1} \\ \hline 0_{N_1 \times N_2} & -\frac{1+\alpha}{N_1} I_{N_2 \times N_2} \end{array} \right], \quad \text{where } N_1 = \frac{N}{d}, \ N_2 = N - N_1,
$$

and A is the Jacobian of the system (2.2) with payoff $B_{N_1,1}$ (simple cycle), mutation (Q1) and evaluated at equilibrium $\boldsymbol{x_{1,1,N_1}} = \frac{1}{N_1} \mathbf{1}_{N_1} = \boldsymbol{x_{mix,N_1}}$.

$M_{N,d}$ has a block diagonal structure with $N - N_1$ eigenvalues equal to $-\frac{1+\alpha}{N_1}$. Its remaining N_1 eigenvalues are given by the eigenvalues of the circulant matrix A. The Jacobian (5.4) evaluated at each of the d equilibria $\boldsymbol{x_{j,d,N}}$ is similar to $M_{N,d}$, hence making the Hopf bifurcation analysis of all of these equilibria equivalent. The matrix A is precisely the Jacobian studied in §4 for the case $N = N_1$ and $\beta = 0$; hence the existence of Hopf bifurcations follows from Theorem 4.5. The criticality of each of these d simultaneous Hopf bifurcations of equilibria $\boldsymbol{x_{j,d,N}}$ is analogous to the criticality calculations in §4.2 and is computed in Appendix E. Corollary 5.2 below summarizes the bifurcation result described above and is the multi-cycle extension to Theorem 4.5. To simplify notation, analogous to (4.4) we set $[A]_{1n} = \gamma_n + \mu\eta_n$.

COROLLARY 5.2. *The system (2.2) with payoff matrix $B_{N,d}$ (with $N \geq 6$, $d = 1, \cdots, N/2$, d a proper divisor of N) and mutation matrix (Q1) has d equilibria $\boldsymbol{x_{j,d,N}}$ ($j = 1, \cdots, d$) that concurrently undergo $\lfloor \frac{N-d}{2d} \rfloor$ Hopf bifurcations, with the rth of such bifurcations located at*

$$
\mu_{0,r} = - \left[\sum_{n=1}^{N/d} \gamma_n \cos\left(\frac{2\pi}{N}(n-1)rd \right) \right] \left[\sum_{n=1}^{N/d} \eta_n \cos\left(\frac{2\pi}{N}(n-1)rd \right) \right]^{-1}
$$

for $r = 1, \cdots, \lfloor \frac{N-d}{2d} \rfloor$, if $\alpha \neq \beta$ and $\mu_{0,r} \neq \frac{\alpha}{2(1+\alpha)}$.

In this section we have shown the coexistence of multiple stable limit cycles for the dynamics, when the underlying circulant payoff graph topologies have multiple distinct cycles. In the following section we investigate the connections between cycles in the payoff graph topology and limit cycles in the dynamics for more general payoff structures.

6. Extensions. Studying the fully general model (2.2), even with $N = 3$ strategies, is highly complex. This complexity motivated our restriction to circulant payoff matrices of the form $B_{C,N}$ (4.1) and $B_{N,d}$ for the analysis in §4 and §5. These results
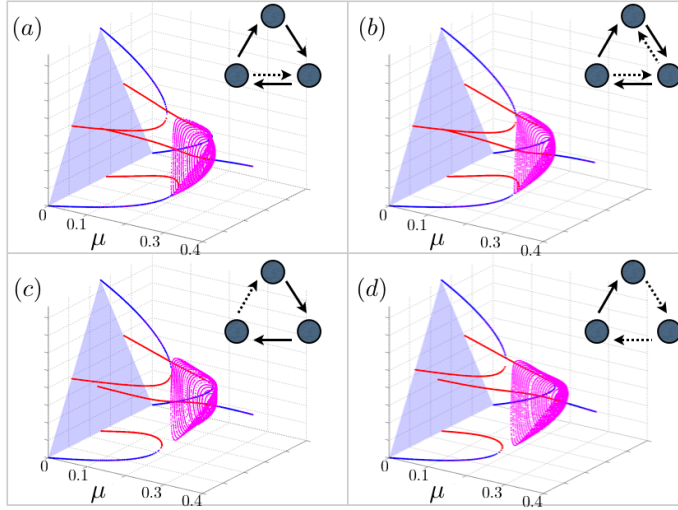

FIG. 6.1. *Limit cycles for noncirculant payoff matrices B, $N = 3$, and mutation matrix* (Q1). *The solid arrows in the graphs are strong links with weight b and the dashed arrows are weak links with weight ϵb. Parameters for all plots are $b = 0.2$ and $\epsilon = 0.1$.*

might lead one to conclude that the circulant structure of payoff matrix B is a *necessary* condition for Hopf bifurcations of the dynamics. In this section we illustrate that this is not the case. We show examples of limit cycles for selected noncirculant payoff matrices, first for $N = 3$ strategies, and then for $N \geq 4$. The simulations in this section illustrate a tight connection between the topology of the payoff graphs and the existence of stable limit cycles for the dynamics. In particular, embedded cycles in the payoff graph appear to be necessary for (and often lead to) the existence of limit cycles, and amplitude and frequency of limit cycles appear to be related to symmetries in the graph.

Consider 3×3 payoff matrices B satisfying (2.1) and Condition 1 that have directed links of two kinds: strong links with weights b and weak links with weights ϵb where $b \in (0, 1)$ and $0 < \epsilon \ll 1$. There are 73 corresponding non-isomorphic graph topologies in the set [22]. Figure 6.1 shows stable limit cycles for four topologies in this set corresponding to noncirculant payoff matrices. Each of these topologies has an embedded directed cycle.

We next look at selected noncirculant payoff topologies with $N \geq 4$ nodes in Figure 6.2. The bifurcation plots (middle panel in Figure 6.2) are obtained by simulating the dynamics for a range of different values of mutation parameter μ and random initial conditions. Stable equilibria are marked blue and limit cycles are marked magenta. Also shown in the right panel of the figure are limit cycle trajectories of the
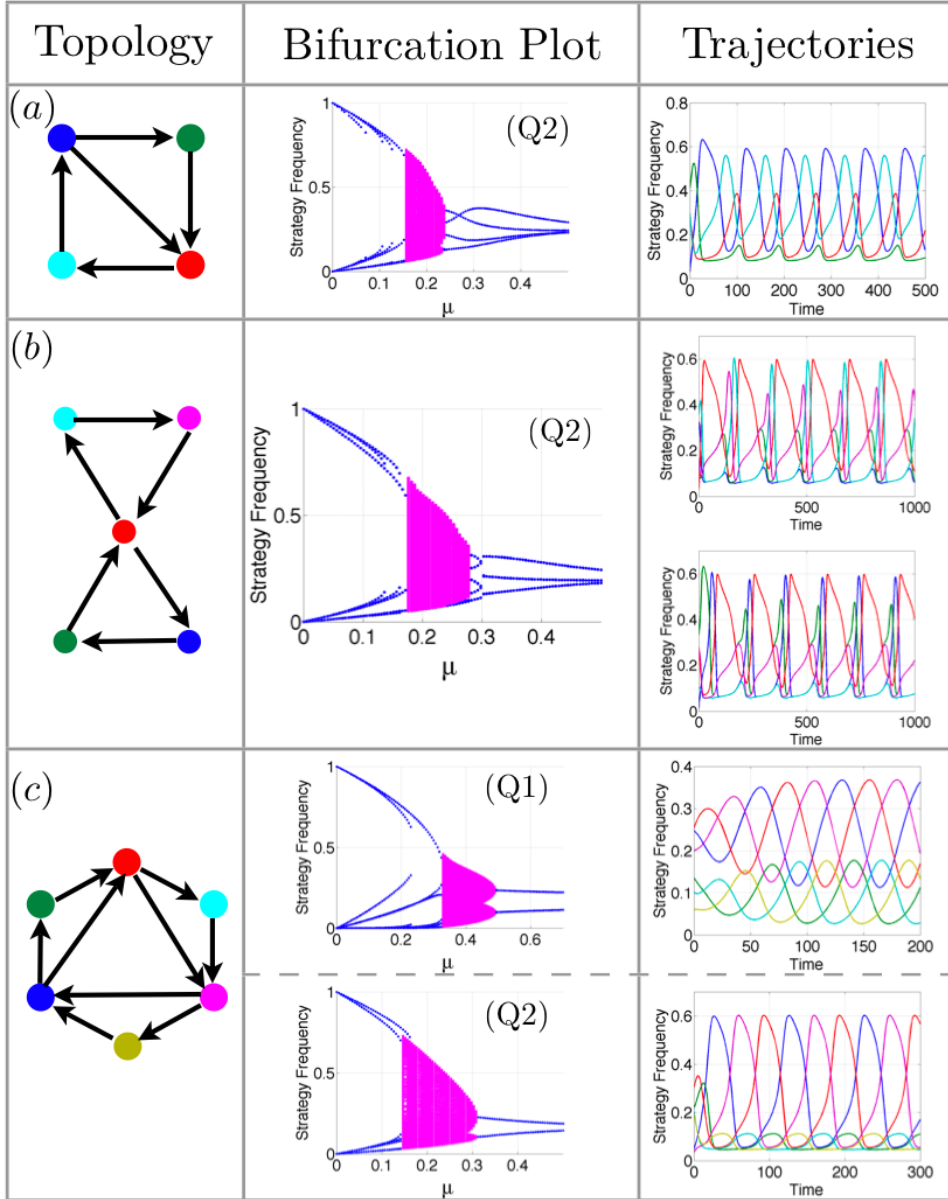
FIG. 6.2. *Limit cycles for the dynamics* (2.2) *with noncirculant payoff graph topology. The left panel shows the payoff graph; all edges have equal weight* $b = 0.7$. *The center panel show the bifurcation plot for each topology and mutation matrix* (Q1) *or* (Q2) *as indicated. The bifurcation plot is obtained by simulating the dynamics for 120 values of the mutation parameter* μ *in the range shown on the x-axis of each plot. For each* μ, *the dynamics are simulated for 12 randomly chosen initial conditions and the limiting set (stable equilibria or limit cycles) is obtained. Stable equilibria are plotted in blue and limit cycles are plotted in magenta. The right panel shows trajectory plots of the dynamics for a value of* μ *chosen in the magenta (limit cycle) range of the bifurcation plot* ($\mu = 0.2$ *in (a), (b) and (c)* (Q2); $\mu = 0.4$ *in (c)* (Q1)). *The colors of each trajectory match the colors of the nodes on the corresponding payoff graph. For topology (b), the two trajectory plots correspond to different initial conditions.*

dynamics for specific chosen values of μ in the magenta range. The colors of the nodes in the topologies (left panel) match the colors of the corresponding trajectories.

Several interesting features can be observed in the plots in Figure 6.2. In topology (a), the connection between the amplitude of oscillation of a given strategy in the trajectory plot and the location of the corresponding node on the graph is apparent. In particular, the cyan node, which is part of two directed cycles, has a significantly higher oscillation amplitude than the green node, which is part of only one directed cycle. The symmetry of topology (b) about the red node leads to the existence of two stable limit cycle attractors, much like the illustrations in §5. On the other hand, topology (c) has two embedded cycles but only one limit cycle attractor for both (Q1) and (Q2) mutation matrices.
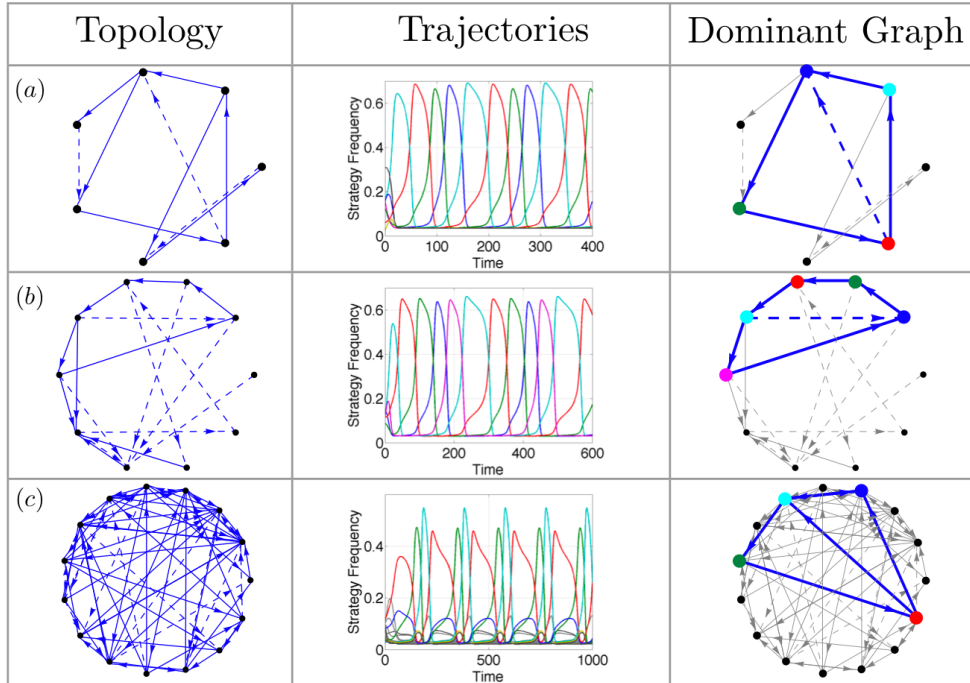
FIG. 6.3. *Limit cycles for the dynamics* (2.2) *with random payoff graphs. The left panel shows the payoff graph with two types of edges:* strong *edges (solid lines) with a weight of b and* weak *edges (dashed lines) with a weight of ϵb; here $b = 0.7$ and $\epsilon = 0.1$. The center panel shows the resulting trajectories with mutation* (Q2) *and suitable μ (0.2 in (a), 0.25 in (b) and 0.27 in (c)). The right panel highlights the interconnection between nodes corresponding to the dominant components of the limit cycle trajectories. The color of each of the nodes on the payoff graph matches the color of the corresponding trajectory in the center panel. In each case, it is observed that there is a directed cycle between the dominant component nodes.*

In Figure 6.3, we go a little further and consider random payoff graph topologies having strong links with weight b and weak links with payoff ϵb, much like in Figure 6.1. We simulate the dynamics for a set of different random graphs and a range of values for the mutation parameter μ, and focus specifically on graphs and parameters that induce a limit cycle oscillation for the dynamics. We show three such examples in Figure 6.3. For each set of simulated limit cycle trajectories, the dominant components are obtained; dominant components are defined as those having a relatively high oscillation amplitude or correspondingly a trajectory with standard deviation above

a set threshold. The main observation we make here is that the existence of limit cycles for the dynamics is tied to the existence of a directed cycle between nodes of the payoff graph. In all our simulations of random graphs, for both mutation matrices (Q1) and (Q2), we consistently find that the dominant components of stable limit cycles correspond to the existence of at least one directed cycle between the corresponding nodes of the payoff graph, as illustrated in the right panel of Figure 6.3.

The purpose of the simulations in this section is to illustrate that one can break symmetry in the payoff graph significantly (as compared to the modest symmetry breaking that yields the circulant structures analyzed in this paper) and get stable limit cycles for the dynamics, even in the case of random graph topologies, as long as the topologies have at least one embedded cycle. In addition to limit cycles, the dynamics can also have chaotic attractors as studied in [15, 16]. We have not seen chaotic attractors for the payoff topologies and mutation matrices (Q1) and (Q2) studied in this paper; we conjecture that studying alternative mutation models as the one used in [16] will yield chaotic dynamics.

7. Final Remarks. The replicator-mutator dynamics define a canonical model from evolutionary theory and have been recently applied to model the evolution of language. The dynamics also provide a simple model for the analysis of behavior dominance in social networks where replication is akin to imitation of individuals subscribed to successful behaviors in a population, and mutation is akin to random error in behavior selection. In networked multi-agent systems, the dynamics model the exploration versus exploitation tradeoff.

Much of the existing analysis of the replicator-mutator dynamics has been focused on stable equilibrium limiting behavior. The analysis in the literature has also primarily considered payoff and mutation matrices that are symmetric, which correspond to undirected payoff graph topologies. Recent work [14] on a graph theoretic model of language dynamics has shown that the graph connectivity plays a critical role in determining the location of bifurcation points in the dynamics, but the restriction to undirected graphs confines the range of limiting behavior to stable equilibria. In [16], it is shown that considering asymmetric payoff and mutation matrices (corresponding to directed graphs) can yield limit cycle behavior and even chaos for replicator-mutator dynamics.

Here we prove conditions such that stable limit cycles in the replicator-mutator dynamics arise as a consequence of Hopf bifurcations for $N \geq 3$ strategies and circulant payoff matrices. From a graph perspective, we show how breaking symmetry by considering directed graphs allows for oscillatory limiting behavior. We emphasize that the limit cycles are not restricted to circulant payoffs, but can exist for noncirculant payoffs as shown in §6. The simulations in §6 illustrate the connection between embedded directed cycles in the payoff graph and the existence of stable limit cycles for the dynamics. A Hopf bifurcation analysis of these more general cases is an intended future direction. We also intend to explore the effect of the structure of the mutation matrix, beyond (Q1) and (Q2) considered here, as a step towards understanding the transition to chaos illustrated in [16].

A further future direction is the application of such evolutionary models to the design of decision-making protocols in multi-agent robotic systems. In this case the mutation parameter μ can be interpreted as a controlled design term that can be varied to get a range of emergent system-level behavior, including dominance, oscillations and mixed collapse.

Appendix A. Proof of Lemma 4.2.

Proof. To simplify notation in this proof, we denote the Jacobian $D_{\boldsymbol{x}}\boldsymbol{g}|_{\boldsymbol{x}_{mix,N}}$ as matrix A. Since A is circulant, its eigenvalues are given by (4.3). From (4.3) we see that the eigenvalue $\lambda_k(A)$ cannot be complex when ω_N^k is real. To guarantee complex ω_N^k let k be given by

$$k \in \begin{cases} \{1, \cdots, N-1\} & N \text{ odd} \\ \{1, \cdots, N-1\} \setminus \{\frac{N}{2}\} & N \text{ even.} \end{cases}$$

One can verify that $\lambda_{N-k}(A) = \overline{\lambda_k(A)}$. Hence, as long as the $\lambda_k(A)$ are complex, A has $\left\lfloor \frac{N-1}{2} \right\rfloor$ complex conjugate pairs of eigenvalues. Now we compute $\mathrm{Im}\,(\lambda_k(A))$ and hence obtain conditions for the existence of complex $\lambda_k(A)$. The calculations differ slightly between mutation matrices (Q1) and (Q2) as shown below. We obtain a simplified expression for the imaginary component of the eigenvalues by grouping identical terms of A and using the identity $\sum_{j=1}^{N} \omega_N^{jk} = 0$.

- Mutation (Q1):

$$\mathrm{Im}\,(\lambda_k(A)) = \begin{cases} (a_{12} - a_{1N}) \sin\left(\frac{2\pi}{N}k\right) & N = 3, 4, 5 \\ (a_{12} - a_{1N}) \sin\left(\frac{2\pi}{N}k\right) + (a_{13} - a_{1,N-1}) \sin\left(\frac{2\pi}{N}2k\right) & N \geq 6 \end{cases}$$

- Mutation (Q2):

$$\mathrm{Im}\,(\lambda_k(A)) = (a_{12} - a_{1N}) \sin\left(\frac{2\pi}{N}k\right) \qquad\qquad N \geq 3$$

Substituting for the a_{ij} terms from (4.2),

$$\mathrm{Im}\,(\lambda_k(A)) = 0 \iff \begin{cases} (\alpha - \beta)\left(1 - \mu - \mu\frac{(2+\alpha+\beta)}{\alpha+\beta}\right) = 0 & \text{mutation (Q1)} \\ (\alpha - \beta)\left(1 - \mu - \frac{\mu}{N-1}\right) = 0 & \text{mutation (Q2).} \end{cases} \tag{A.1}$$

The conditions of the Lemma follow from the expressions in (A.1). □

Appendix B. First Lyapunov Coefficient. As stated in Theorem 4.3, the sign of the *first Lyapunov coefficient* $\ell_1|_{(\boldsymbol{x}_0,\mu_0)}$ evaluated at the fixed point $\boldsymbol{x}_0$ and bifurcation point μ_0 determines the criticality of the Hopf bifurcation. What follows are the expressions for calculating $\ell_1|_{(\boldsymbol{x}_0,\mu_0)}$ as presented in [13].

Consider the N-dimensional dynamical system $\dot{\boldsymbol{x}} = \boldsymbol{f}(\boldsymbol{x},\mu)$ where $\boldsymbol{x} \in \mathbb{R}^N$ and $\mu \in \mathbb{R}$. Let $A_0 = D_{\boldsymbol{x}}\boldsymbol{f}|_{(\boldsymbol{x}_0,\mu_0)}$, where $\boldsymbol{x}_0 \in \mathbb{R}^N, \mu_0 \in \mathbb{R}$. A_0 has two purely imaginary complex conjugate eigenvalues, given by $\pm\mathbf{i}\,\omega_0$, where $\omega_0 > 0$. Define T_1, T_2 and T_3 as

$$\begin{aligned} T_1 &= \langle \boldsymbol{p}, \mathfrak{C}\,(\boldsymbol{q},\boldsymbol{q},\overline{\boldsymbol{q}}) \rangle \\ T_2 &= \left\langle \boldsymbol{p}, \mathfrak{B}\left(\overline{\boldsymbol{q}}, (2\mathbf{i}\,\omega_0 - A_0)^{-1}\,\mathfrak{B}\,(\boldsymbol{q},\boldsymbol{q})\right) \right\rangle \\ T_3 &= -2 \left\langle \boldsymbol{p}, \mathfrak{B}\left(\boldsymbol{q}, A_0^{-1}\mathfrak{B}\,(\boldsymbol{q},\overline{\boldsymbol{q}})\right) \right\rangle. \end{aligned}$$

Here $\langle \boldsymbol{r}, \boldsymbol{s} \rangle = \overline{\boldsymbol{r}} \cdot \boldsymbol{s}$ is the complex inner product between two complex vectors, and $\boldsymbol{q}$ and $\boldsymbol{p}$ are respectively the normalized eigenvector and adjoint-eigenvector of A_0

satisfying $A_0 \boldsymbol{q} = \mathbf{i}\,\omega_0 \boldsymbol{q}$, $A_0^T \boldsymbol{p} = -\mathbf{i}\,\omega_0 \boldsymbol{p}$, and normalization $\langle \boldsymbol{p}, \boldsymbol{q} \rangle = 1$. $\mathfrak{B}$ and $\mathfrak{C}$ are high dimensional tensors given by

$$
\mathfrak{B}(\boldsymbol{r}, \boldsymbol{s}) = \begin{bmatrix} \mathfrak{B}_1(\boldsymbol{r}, \boldsymbol{s}) \\ \mathfrak{B}_2(\boldsymbol{r}, \boldsymbol{s}) \\ \vdots \\ \mathfrak{B}_N(\boldsymbol{r}, \boldsymbol{s}) \end{bmatrix}, \; \mathfrak{B}_i(\boldsymbol{r}, \boldsymbol{s}) = \sum_{k,l} \left. \frac{\partial^2 f_i}{\partial x_k \partial x_l} \right|_{\boldsymbol{x}=\boldsymbol{x}_0} r_k s_l
$$

$$
\mathfrak{C}(\boldsymbol{r}, \boldsymbol{s}, \boldsymbol{t}) = \begin{bmatrix} \mathfrak{C}_1(\boldsymbol{r}, \boldsymbol{s}, \boldsymbol{t}) \\ \mathfrak{C}_2(\boldsymbol{r}, \boldsymbol{s}, \boldsymbol{t}) \\ \vdots \\ \mathfrak{C}_N(\boldsymbol{r}, \boldsymbol{s}, \boldsymbol{t}) \end{bmatrix}, \; \mathfrak{C}_i(\boldsymbol{r}, \boldsymbol{s}, \boldsymbol{t}) = \sum_{k,l,m} \left. \frac{\partial^3 f_i}{\partial x_k \partial x_l \partial x_m} \right|_{\boldsymbol{x}=\boldsymbol{x}_0} r_k s_l t_m
$$

The first Lyapunov coefficient $\ell_1|_{(\boldsymbol{x}_0, \mu_0)}$ is given by

$$
\ell_1|_{(\boldsymbol{x}_0, \mu_0)} = \frac{1}{2\omega_0} \mathrm{Re}\left(T_1 + T_2 + T_3\right).
$$

Appendix C. Proof of Lemma 4.4.

Proof. To simplify notation in this proof, we denote the Jacobian $D_{\boldsymbol{x}} \boldsymbol{g}|_{\boldsymbol{x}_{mix}, N}$ as matrix A. From Lemma 4.2, for $r = 1, \cdots, \lfloor \frac{N-1}{2} \rfloor$, $\lambda_r(A)$ is complex. Using the notation $a_{1j} = \gamma_j + \mu \eta_j$ we obtain

$$
\mathrm{Re}\left(\lambda_r(A)\right) = \sum_{j=1}^{N} \gamma_j \cos\left(\frac{2\pi}{N}(j-1)r\right) + \mu \sum_{j=1}^{N} \eta_j \cos\left(\frac{2\pi}{N}(j-1)r\right)
$$

which is zero if and only if

$$
\mu = -\left[\sum_{j=1}^{N} \gamma_j \cos\left(\frac{2\pi}{N}(j-1)r\right)\right] \left[\sum_{j=1}^{N} \eta_j \cos\left(\frac{2\pi}{N}(j-1)r\right)\right]^{-1} =: \mu_{0,r}. \quad \text{(C.1)}
$$

Before we proceed, we need to establish that $\mu_{0,r}$ is indeed well defined; that is, the denominator in (C.1) is non-zero. Let d_r denote the denominator of $\mu_{0,r}$. For $N = 3$, $d_r = 6(\alpha + \beta + \alpha\beta) \neq 0$ for mutation (Q1) and $d_r = 3(4 + \alpha + \beta) \neq 0$ for mutation (Q2); for $N = 4$, $d_r = 2(\alpha + \beta + 2\alpha\beta) \neq 0$ for mutation (Q1) and $d_r = 4(2 + \alpha + \beta) \neq 0$ for mutation (Q2). For $N \geq 5$, by grouping identical terms, using the identity $\sum_{j=1}^{N} \omega_N^{jr} = 0$ and replacing the expressions for η_j in terms of α and β we have,

$$
d_r \neq 0 \iff \begin{cases} 2(\alpha + \beta)\left(\cos\left(\frac{2\pi}{N}r\right) - 1\right) + 2\alpha\beta\left(\cos\left(\frac{2\pi}{N}2r\right) - 1\right) \neq 0 & \text{mutation (Q1)} \\ \cos\left(\frac{2\pi}{N}r\right) \neq -\frac{2+\alpha+\beta}{\alpha+\beta} & \text{mutation (Q2).} \end{cases}
$$

The conditions above can be verified to always hold given that the cosine function is bounded between -1 and 1 and α and β satisfy the conditions in (4.1).

Finally, we establish that if $r, s = 1, \cdots \lfloor \frac{N-1}{2} \rfloor$, $r \neq s$ then $\mu_{0,r} \neq \mu_{0,s}$, i.e. the bifurcation points are distinct. If $N = 3, 4$, Lemma 4.2 establishes that there is only one bifurcation point. For $N = 5$, the two critical points can be shown to be distinct

by a direct calculation. Here we show the distinctness of the critical points in the cases $N \geq 6$. Using (C.1),

$$\mu_{0,r} \neq \mu_{0,s} \iff \frac{\sum_{j=1}^{N} \gamma_j \cos\left(\frac{2\pi}{N}(j-1)r\right)}{\sum_{j=1}^{N} \eta_j \cos\left(\frac{2\pi}{N}(j-1)r\right)} \neq \frac{\sum_{j=1}^{N} \gamma_j \cos\left(\frac{2\pi}{N}(j-1)s\right)}{\sum_{j=1}^{N} \eta_j \cos\left(\frac{2\pi}{N}(j-1)s\right)}. \tag{C.2}$$

By grouping identical terms, using the identity $\displaystyle\sum_{j=1}^{N} \omega_N^{jr} = 0$ and replacing the expressions for γ_j and η_j in terms of α and β,

$$(\text{C.2}) \iff \begin{cases} (1+\alpha+\beta+2\alpha\beta)(\alpha+\beta) \\ +2\alpha\beta\left[\cos\left(\frac{2\pi}{N}r\right) + \cos\left(\frac{2\pi}{N}s\right)\right] \\ +2(\alpha+\beta)\alpha\beta\left[\cos\left(\frac{2\pi}{N}r\right)\cos\left(\frac{2\pi}{N}s\right)\right] \neq 0 \quad \text{mutation (Q1)} \\ \\ \cos\left(\frac{2\pi}{N}r\right) \neq \cos\left(\frac{2\pi}{N}s\right) \qquad\qquad\qquad\quad \text{mutation (Q2)} \end{cases} \tag{C.3}$$

For mutation (Q1), the left hand side of the inequality in (C.3) can be bounded below by $(\alpha - \beta)^2 + (\alpha + \beta) > 0$. For mutation (Q2), the condition in (C.3) is equivalent to the initial hypothesis of $r \neq s$. The distinctness result now follows. □

Appendix D. Proof of Lemma 4.6.

Proof. Here we compute the terms T_1, T_2 and T_3 from Appendix B to obtain a simplified analytical expression for the first Lyapunov coefficient $\ell_1|_{(\boldsymbol{x_{mix,N}}, \mu_{0,r})}$. For a circulant matrix $M \in \mathbb{R}^{N \times N}$, let $\{(\lambda_k, \boldsymbol{v_k})\}$ be an eigenvalue–right eigenvector pair $(M\boldsymbol{v_k} = \lambda_k \boldsymbol{v_k})$, where

$$\boldsymbol{v_k} = \begin{bmatrix} 1 & \omega_N^k & \omega_N^{2k} & \cdots & \omega_N^{(N-1)k} \end{bmatrix}^T \quad \text{and} \quad \lambda_k(M) = \sum_{j=1}^{N} m_{1j}\, \omega_N^{(j-1)k}. \tag{D.1}$$

We compute $\ell_1|_{(\boldsymbol{x_{mix,N}}, \mu_{0,r})}$ as a function of the parameters α and β. From Appendix B, the Jacobian $D_{\boldsymbol{x}}\boldsymbol{g}|_{(\boldsymbol{x_{mix,N}}, \mu_{0,r})}$ is denoted by A_0 with eigenvalues $\lambda_r(A_0) = \mathbf{i}\,\hat{\omega}$ and $\lambda_{N-r}(A_0) = -\mathbf{i}\,\hat{\omega}$. Let $\omega_0 = |\hat{\omega}|$, $t = r\,\mathrm{sign}(\hat{\omega})$, and $\boldsymbol{q} = \boldsymbol{v_t}$. Note that $A_0\boldsymbol{q} = \mathbf{i}\,\omega_0\boldsymbol{q}$.

Computing T_1. Direct calculation and simplification gives

$$\mathfrak{C}_i(\boldsymbol{q}, \boldsymbol{q}, \overline{\boldsymbol{q}}) = -2N\left[2 + (\alpha+\beta)\,\omega_N^t + (\alpha+\beta)\,\omega_N^{-t}\right]\omega_N^{(i-1)t}.$$

Hence

$$\mathfrak{C}(\boldsymbol{q}, \boldsymbol{q}, \overline{\boldsymbol{q}}) = -2N\left[2 + (\alpha+\beta)\,\omega_N^t + (\alpha+\beta)\,\omega_N^{-t}\right]\boldsymbol{q},$$

which leads to

$$\begin{aligned} T_1 = \langle \boldsymbol{p}, \mathfrak{C}(\boldsymbol{q}, \boldsymbol{q}, \overline{\boldsymbol{q}}) \rangle &= -2N\left[2 + (\alpha+\beta)\,\omega_N^t + (\alpha+\beta)\,\omega_N^{-t}\right]\langle \boldsymbol{p}, \boldsymbol{q} \rangle \\ &= -2N\left[2 + (\alpha+\beta)\left(\omega_N^t + \omega_N^{-t}\right)\right]. \end{aligned} \tag{D.2}$$

Computing T_2. We compute

$$\mathfrak{B}(\boldsymbol{q}, \boldsymbol{q}) = 2\left[1 + \alpha\omega_N^t + \beta\omega_N^{-t}\right] Q^T \boldsymbol{v}_{2t}.$$

Since Q is circulant, so is Q^T and $\boldsymbol{v}_{2t}$ is a right eigenvector. Then

$$\mathfrak{B}(\boldsymbol{q}, \boldsymbol{q}) = 2\left[1 + \alpha\omega_N^t + \beta\omega_N^{-t}\right] \lambda_{2t}\left(Q^T\right) \boldsymbol{v}_{2t}.$$

For each eigenvalue-eigenvector pair $\lambda, \boldsymbol{v}$ of A_0, $1/\left(2\mathbf{i}\,\omega_0 - \lambda\right)$ is the corresponding eigenvalue for the eigenvector $\boldsymbol{v}$ of $\left(2\mathbf{i}\,\omega_0 I - A_0\right)^{-1}$, where I denotes the identity matrix. Then,

$$\left(2\mathbf{i}\,\omega_0 I - A_0\right)^{-1}\mathfrak{B}(\boldsymbol{q}, \boldsymbol{q}) = 2\frac{\left[1 + \alpha\omega_N^t + \beta\omega_N^{-t}\right] \lambda_{2t}\left(Q^T\right)}{2\mathbf{i}\,\omega_0 - \lambda_{2t}\left(A_0\right)}\boldsymbol{v}_{2t}.$$

Since $\mathfrak{B}(\boldsymbol{x}, \kappa\boldsymbol{y}) = \kappa\mathfrak{B}(\boldsymbol{x}, \boldsymbol{y})$ for any $\kappa \in \mathbb{C}$, then

$$\mathfrak{B}\left(\overline{\boldsymbol{q}}, \left(2\mathbf{i}\,\omega_0 - A_0\right)^{-1}\mathfrak{B}(\boldsymbol{q}, \boldsymbol{q})\right) = 2\frac{\left[1 + \alpha\omega_N^t + \beta\omega_N^{-t}\right] \lambda_{2t}\left(Q^T\right)}{2\mathbf{i}\,\omega_0 - \lambda_{2t}\left(A_0\right)}\mathfrak{B}\left(\overline{\boldsymbol{q}}, \boldsymbol{v}_{2t}\right).$$

A calculation similar to that for $\mathfrak{B}(\boldsymbol{q}, \boldsymbol{q})$ gives

$$\mathfrak{B}_i\left(\overline{\boldsymbol{q}}, \boldsymbol{v}_{2t}\right) = \left[\beta\omega_N^{-2t} + \alpha\omega_N^{-t} + 2 + \beta\omega_N^t + \alpha\omega_N^{2t}\right]\sum_{j=1}^N q_{ji}\,\omega_N^{(j-1)t}.$$

Hence

$$\mathfrak{B}\left(\overline{\boldsymbol{q}}, \boldsymbol{v}_{2t}\right) = \left(\beta\omega_N^{-2t} + \alpha\omega_N^{-t} + 2 + \beta\omega_N^t + \alpha\omega_N^{2t}\right)\lambda_t\left(Q^T\right)\boldsymbol{q}.$$

This implies

$$\mathfrak{B}\left(\overline{\boldsymbol{q}}, \left(2\mathbf{i}\,\omega_0 - A_0\right)^{-1}\mathfrak{B}(\boldsymbol{q}, \boldsymbol{q})\right)$$
$$= \frac{2\lambda_t\left(Q^T\right)\lambda_{2t}\left(Q^T\right)}{2\mathbf{i}\,\omega_0 - \lambda_{2t}\left(A_0\right)}\left(1 + \alpha\omega_N^t + \beta\omega_N^{-t}\right)\left[\beta\omega_N^{-2t} + \alpha\omega_N^{-t} + 2 + \beta\omega_N^t + \alpha\omega_N^{2t}\right]\boldsymbol{q}$$

and

$$T_2 = \left\langle \boldsymbol{p}, \mathfrak{B}\left(\overline{\boldsymbol{q}}, \left(2\mathbf{i}\,\omega_0 - A_0\right)^{-1}\mathfrak{B}(\boldsymbol{q}, \boldsymbol{q})\right)\right\rangle$$
$$= \frac{2\lambda_t\left(Q^T\right)\lambda_{2t}\left(Q^T\right)}{2\mathbf{i}\,\omega_0 - \lambda_{2t}\left(A_0\right)}\left(1 + \alpha\omega_N^t + \beta\omega_N^{-t}\right)\left[\beta\omega_N^{-2t} + \alpha\omega_N^{-t} + 2 + \beta\omega_N^t + \alpha\omega_N^{2t}\right]. \quad \text{(D.3)}$$

Computing T_3. We show that $\mathfrak{B}(\boldsymbol{q}, \overline{\boldsymbol{q}}) = \mathbf{0}$.

$$\mathfrak{B}_i(\boldsymbol{q}, \overline{\boldsymbol{q}}) = -2 - (\alpha + \beta)\left(\omega_N^t + \omega_N^{-t}\right) + \left[2 + (\alpha + \beta)\left(\omega_N^t + \omega_N^{-t}\right)\right]\sum_{j=1}^N q_{ji}$$

$$= \left[2 + (\alpha + \beta)\left(\omega_N^t + \omega_N^{-t}\right)\right]\left[-1 + \sum_{j=1}^N q_{ji}\right] = 0, \quad \text{(D.4)}$$

where the last equality comes from the fact that Q is a doubly-stochastic matrix. This implies

$$T_3 = -2 \left\langle \boldsymbol{p}, \mathfrak{B} \left(\boldsymbol{q}, A_0^{-1} \mathfrak{B} \left(\boldsymbol{q}, \overline{\boldsymbol{q}} \right) \right) \right\rangle = -2 \left\langle \boldsymbol{p}, \mathfrak{B} \left(\boldsymbol{q}, \boldsymbol{0} \right) \right\rangle = 0.$$

Combining the previous expressions for T_1, T_2 and T_3, the result follows.   □

Appendix E. Criticality analysis for Corollaries 5.1 and 5.2.

In this section we establish that the Lyapunov coefficient at each of the d concurrent Hopf Bifurcations of the equilibria $\boldsymbol{x_{j,d,N}}$ is identical to that at the equilibrium $\boldsymbol{x_{mix,N/d}}$ for the simple cycle payoff $B_{C,N/d}$ with $\beta = 0$ (i.e. $B_{N/d,1}$). The mutation matrix used is (Q1). Let $N/d = N_1$ and $N_2 = N - N_1$.

In order to simplify the calculations, consider the payoff matrix $\hat{B}_{N,d}$ given by

$$\hat{B}_{N,d} = \left[\begin{array}{c|c|c|c} B_{N_1,1} & 0_{N_1 \times N_1} & \cdots & 0_{N_1 \times N_1} \\ \hline 0_{N_1 \times N_1} & B_{N_1,1} & \cdots & 0_{N_1 \times N_1} \\ \hline \vdots & \vdots & \ddots & \vdots \\ \hline 0_{N_1 \times N_1} & 0_{N_1 \times N_1} & \cdots & B_{N_1,1} \end{array} \right].$$

$\hat{B}_{N,d}$ is obtained by relabeling the graph nodes corresponding to $B_{N,d}$ such that index labels for connected nodes are consecutive. The payoff graph topology induced by $\hat{B}_{N,d}$ is isomorphic to that of $B_{N,d}$, see Figure 5.1. The dynamics (2.2), with payoff $\hat{B}_{N,d}$ and mutation (Q1) have equilibria $\hat{\boldsymbol{x}}_{\boldsymbol{j}} = \left[\boldsymbol{0}_{N_1(j-1)}^T \quad \frac{1}{N_1} \boldsymbol{1}_{N_1}^T \quad \boldsymbol{0}_{N_1(d-j)}^T \right]^T$, which correspond to the equilibria $\boldsymbol{x_{j,d,N}}$. The Jacobian of the system above evaluated at the equilibrium $\hat{\boldsymbol{x}}_{\boldsymbol{1}}$ is precisely $M_{N,d}$ in (5.3). Using this definition of payoff, we compute the first Lyapunov coefficient as described in Appendix B. We focus on equilibrium $\hat{\boldsymbol{x}}_{\boldsymbol{1}}$; the analysis for the other $\hat{\boldsymbol{x}}_{\boldsymbol{j}}$ is equivalent.

The eigenvalues λ_k and eigenvectors $\boldsymbol{v}_k$ of a circulant matrix are defined in (D.1). Let the Jacobian $M_{N,d}$ evaluated at the critical point $\mu_{0,r}$ (defined in Corollary 5.2) be denoted as

$$\hat{A}_0 = \left[\begin{array}{c|c} A_0 & 0_{N_2 \times N_1} \\ \hline 0_{N_1 \times N_2} & -\frac{1+\alpha}{N_1} I_{N_2 \times N_2} \end{array} \right],$$

with a purely complex conjugate pair of eigenvalues $\lambda_r(A_0) = \mathbf{i}\,\hat{\omega}$ and $\lambda_{N-r}(A_0) = -\mathbf{i}\,\hat{\omega}$. Let $\omega_0 = |\hat{\omega}|$, $t = r\,\mathrm{sign}(\hat{\omega})$, $\boldsymbol{q} = \boldsymbol{v}_t(A_0)$, $\hat{\boldsymbol{q}} = \left[\boldsymbol{q}^T \quad \boldsymbol{0}_{d(N_1-1)}^T \right]^T$ and $\langle \hat{\boldsymbol{p}}, \hat{\boldsymbol{q}} \rangle = 1$. Note that $A_0 \boldsymbol{q} = \mathbf{i}\,\omega_0 \boldsymbol{q}$ and hence $\hat{A}_0 \hat{\boldsymbol{q}} = \mathbf{i}\,\omega_0 \hat{\boldsymbol{q}}$. Let Q be the (Q1) mutation matrix corresponding to $B_{N,d}$ and $\hat{Q}$ be the (Q1) mutation matrix corresponding to $\hat{B}_{N,d}$.

With these definitions, we follow the calculations in Appendix B and compute each of the terms T_1, T_2 and T_3 given below. A comparison of each of these terms, to the corresponding terms in Appendix D shows that the Lyapunov coefficient is identical (when $N \mapsto N_1$, $\beta \mapsto 0$ in (D.2), (D.3) and (D.4)).

$$T_1 = \left\langle \hat{\boldsymbol{p}}, \mathfrak{C}\left(\hat{\boldsymbol{q}}, \hat{\boldsymbol{q}}, \overline{\hat{\boldsymbol{q}}}\right)\right\rangle = -2N_1 \left[2 + \alpha\omega_{N_1}^t + \alpha\omega_{N_1}^{-t}\right]$$

$$T_2 = \left\langle \hat{\boldsymbol{p}}, \mathfrak{B}\left(\overline{\hat{\boldsymbol{q}}}, \left(2\mathbf{i}\,\omega_0 - \hat{A}_0\right)^{-1}\mathfrak{B}\left(\hat{\boldsymbol{q}}, \hat{\boldsymbol{q}}\right)\right)\right\rangle$$

$$= \frac{2\lambda_t\left(Q^T\right)\lambda_{2t}\left(Q^T\right)}{2\mathbf{i}\,\omega_0 - \lambda_{2t}\left(A_0\right)}\left(1 + \alpha\omega_{N_1}^t\right)\left[\alpha\omega_{N_1}^{-t} + \alpha\omega_{N_1}^{2t} + 2\right]$$

$$T_3 = -2\left\langle \hat{\boldsymbol{p}}, \mathfrak{B}\left(\hat{\boldsymbol{q}}, \hat{A}_0^{-1}\mathfrak{B}\left(\hat{\boldsymbol{q}}, \overline{\hat{\boldsymbol{q}}}\right)\right)\right\rangle = 0$$

Acknowledgments. The authors would like to thank two anonymous referees for their helpful comments.

REFERENCES

[1] A.J. Bladon, T. Galla, and A.J. McKane, *Evolutionary dynamics, intrinsic noise, and cycles of cooperation*, Physical Review E, 81 (2010).

[2] R. Bürger, *Mathematical properties of mutation-selection models*, Genetica, 102-103 (1998), pp. 279–298.

[3] W. Garrett Mitchener, *Bifurcation analysis of the fully symmetric language dynamical equation*, Journal of Mathematical Biology, 46 (2003), pp. 265–285.

[4] J. Guckenheimer and P. Holmes, *Nonlinear Oscillations, Dynamical Systems, and Bifurcations of Vector Fields*, Springer, 2002.

[5] K.P. Hadeler, *Stable polymorphisms in a selection model with mutation*, SIAM Journal on Applied Mathematics, (1981), pp. 1–7.

[6] J. Hofbauer and K. Sigmund, *Evolutionary Games and Replicator Dynamics*, Cambridge University Press, 1998.

[7] ———, *Evolutionary game dynamics*, Bulletin of the American Mathematical Society, 40 (2003), p. 479.

[8] R. Horn and C. Johnson, *Matrix Analysis*, Cambridge University Press, 1990.

[9] I. Hussein, *An individual-based evolutionary dynamics model for networked social behaviors*, in Proceedings of the American Control Conference, 2009, pp. 5789–5796.

[10] N.L. Komarova, *Replicator-mutator equation, universality property and population dynamics of learning*, Journal of Theoretical Biology, 230 (2004), pp. 227–239.

[11] N.L. Komarova and S.A. Levin, *Eavesdropping and language dynamics*, Journal of Theoretical Biology, 264 (2010), pp. 104–118.

[12] N.L. Komarova, P. Niyogi, and M.A. Nowak, *The evolutionary dynamics of grammar acquisition*, Journal of Theoretical Biology, 209 (2001), pp. 43–59.

[13] Y. Kuznetsov, *Elements of Applied Bifurcation Theory*, Springer, 1998.

[14] Y. Lee, T. Collier, C. Taylor, and R. Olfati-Saber, *Simplicity from complexity: emergence of cohesion in the evolutionary dynamics of grammar networks*, Evolutionary Ecology, 11 (2009), pp. 433–445.

[15] W. Mitchener, *A Mathematical Model of Human Languages: The interaction of game dynamics & learning processes*, Princeton University, 2003.

[16] W.G. Mitchener and M.A. Nowak, *Chaos and language.*, Proceedings of the Royal Society B: Biological Sciences, 271 (2004), pp. 701–704.

[17] M.A. Nowak, N.L. Komarova, and P. Niyogi, *Evolution of universal grammar*, Science, 291 (2001), p. 114.

[18] M. Nowak and K. Sigmund, *Chaos and the evolution of cooperation*, Proceedings of the National Academy of Sciences, 90 (1993), pp. 5091–5094.

[19] M.A. Nowak and K. Sigmund, *Evolutionary dynamics of biological games*, Science's STKE, 303 (2004), pp. 793–799.

[20] R. Olfati-Saber, *Evolutionary dynamics of behavior in social networks*, in 46th IEEE Conference on Decision and Control, 2007, pp. 4051–4056.

[21] K.M. Page and M.A. Nowak, *Unifying evolutionary dynamics*, Journal of Theoretical Biology, 219 (2002), pp. 93–98.

[22] D. Pais and N.E. Leonard, *Limit cycles in replicator-mutator network dynamics*, in 50th IEEE Conference on Decision and Control, 2011, pp. 3922 –3927.

[23] G.R. Price, *Selection and covariance.*, Nature, 227 (1970), pp. 520–21.

[24] ———, *Extension of covariance selection mathematics*, Annals of human genetics, 35 (1972), pp. 485–490.

[25] J.M. Smith, *Evolution and the Theory of Games*, Cambridge University Press, 1982.

[26] P.F. Stadler and P. Schuster, *Mutation in autocatalytic reaction networks*, Journal of mathematical biology, 30 (1992), pp. 597–632.

[27] P.D. Taylor and L.B. Jonker, *Evolutionary stable strategies and game dynamics*, Mathematical Biosciences, 40 (1978), pp. 145–156.

[28] H. Tembine, E. Altman, R. El-Azouzi, and Y. Hayel, *Evolutionary games in wireless networks*, IEEE Transactions on Systems, Man, and Cybernetics, Part B, 40 (2010), pp. 634–646.

[29] A. Traulsen, J.C. Claussen, and C. Hauert, *Coevolutionary dynamics: from finite to infinite populations*, Physical review letters, 95 (2005).

[30] ———, *Coevolutionary dynamics in large, but finite populations*, Physical Review E, 74 (2006).

[31] T.L. Vincent and J.S. Brown, *Evolutionary game theory, natural selection, and Darwinian dynamics*, Cambridge University Press, 2005.

[32] T.L. Vincent and T.L.S. Vincent, *Evolution and control system design: the evolutionary game*, Control Systems Magazine, IEEE, 20 (2002), pp. 20–35.

[33] Y. Wang and I. Hussein, *Evolutionary bandwidth allocation and routing in large-scale wireless sensor networks*, in Proceedings of the American Control Conference, 2010, pp. 1850–1855.

[34] J.W. Weibull, *Evolutionary Game Theory*, The MIT press, 1997.